Article:
Englong, Apichaya, Punwong, Paramita, Seelanan, Tosak et al. (4 more authors) (2024) Unveiling 4500 years of environmental dynamics and human activity at Songo Mnara, Tanzania. Quaternary Science Advances. 100192. ISSN: 2666-0334

https://doi.org/10.1016/j.qsa.2024.100192

Quaternary Science Advances 14 (2024) 100192

Contents lists available at ScienceDirect

Quaternary Science Advances

journal homepage: www.sciencedirect.com/journal/quaternary-science-advances

Unveiling 4500 years of environmental dynamics and human activity at Songo Mnara, Tanzania

Apichaya Englong [a,b], Paramita Punwong [c,d,*], Tosak Seelanan [b,**], Rob Marchant [d], Stephanie Wynne-Jones [e], Akkaneewut Jirapinyakul [f], Jeffrey Fleisher [g]

[a] Biological Sciences Program, Faculty of Science, Chulalongkorn University, Bangkok, 10330, Thailand
[b] Plants of Thailand Research Unit, Department of Botany, Faculty of Science, Chulalongkorn University, Bangkok, 10330, Thailand
[c] Faculty of Environment and Resource Studies, Mahidol University, Salaya, Phutthamonthon, Nakhon Pathom, 73170, Thailand
[d] York Institute of Tropical Ecosystems, Department of Environment and Geography, University of York, York, YO105NG, UK
[e] Department of Archaeology, University of York, York, UK
[f] Center of Excellence for the Morphology of Earth Surface and Advanced Geohazards in Southeast 13 Asia (MESA CE), Department of Geology, Faculty of Science, Chulalongkorn University, 14 Patumwan, Bangkok, 10330, Thailand
[g] Department of Anthropology, Rice University, Houston, TX, 77005, USA

ARTICLE INFO

Keywords:
Palaeoenvironment
Sea-level change
Pollen analysis
Human-environment interaction

ABSTRACT

Coastal East Africa has undergone massive transformations through the Late Holocene, with a combination of changes in sea level, increasing human settlement, and ensuing use of coastal resources. A comprehensive multi-proxy analysis, including pollen, phytolith, charcoal, stratigraphy, particle size, and geochemical data from sedimentary cores extracted from mangrove ecosystems combined with soils from archaeological contexts, provided valuable insights into vegetation dynamics, environmental changes, and human interactions within the mangrove ecosystem of Songo Mnara Island, Tanzania over the last 2590 BCE (4540 cal yr BP). The bottommost layers indicate a lack of vegetation, as deduced from the presence of coral rags and high calcium and carbonate content, possibly due to high mid-Holocene sea-level. Evidence of mangrove taxa suggests a decrease in sea level, enabling the establishment of mangroves from around 2590 BCE. A brief period of sea-level rise occurred between 90 BCE and 320 CE before sea-level fell until 1570 CE. Significant evidence of human activity is recorded from around 1400 CE indicated by increased charcoal, crop phytoliths, and evidence of marine resource utilisation. The timing of this human-environment interaction is also linked to the time of lower sea level. However, there was evidence suggesting human abandonment of the island from around 1500 CE. This coincided with a subsequent rise in sea levels and potentially prolonged drought conditions spanning from 1570 to 1700 CE. These factors likely contributed to a shortage of food resources in the area, impacting both agricultural practices due to the scarcity of natural freshwater and the accessibility of marine food resources. From 1700 CE to the present, fluctuations in sea level have been observed, with a signal of recent sea-level rise in tandem with shifts in mangrove, terrestrial herbaceous taxa and fire activity.

The low sedimentation rates within mangrove areas suggest that the mangroves on Songo Mnara Island may not keep pace with the current rate of sea-level rise.

1. Introduction

Mangrove ecosystems, transitional between terrestrial and marine environments, have experienced dynamic changes attributed to climatic and relative sea-level fluctuations (Cohen et al., 2021; Fontes et al., 2017; Moraes et al., 2021). These factors shape mangrove ecological dynamics and adaptive responses to environmental changes. Mangroves respond to sea-level changes by migrating seaward during falling sea levels, and expanding landward during rising sea levels (Gilman et al., 2008). Accumulating sediment and preserving fossils, mangroves offer insights into sea-level changes, freshwater input, and compositional shifts (Bozi et al., 2021; Cohen et al., 2021; Ellison, 2015; Punwong

* Corresponding author. Faculty of Environment and Resource Studies, Mahidol University, Salaya, Phutthamonthon, Nakhon Pathom, 73170, Thailand.
** Corresponding author. Plants of Thailand Research Unit, Department of Botany, Faculty of Science, Chulalongkorn University, Bangkok, 10330, Thailand.
E-mail addresses: paramita.pun@mahidol.edu (P. Punwong), tosak.s@chula.ac.th (T. Seelanan).

https://doi.org/10.1016/j.qsa.2024.100192
Received 13 October 2023; Received in revised form 18 March 2024; Accepted 2 May 2024
Available online 3 May 2024

et al., 2024). Crucial for tracking past environmental shifts and human-mangrove interactions; understanding historical mangrove dynamics aids in anticipating their response to future sea-level changes (Gilman et al., 2008).

Research on mangrove ecosystems along the Tanzanian coast is limited and primarily focused on Zanzibar (Englong et al., 2023; Punwong et al., 2013a, 2013c, 2013b, 2018a). Although Zanzibar was an important centre, the Swahili coast encompasses the whole Kenyan and Tanzanian coast. Swahili culture were historically very significant in terms of trade, culture, architecture and maritime skills (Wynne-Jones and LaViolette, 2017). Notably, Swahili settlements and coastal trading ports were often established near mangrove areas. These mangrove ecosystems provided crucial resources, including marine food and construction materials, for the Swahili people; playing a significant role in the development of Swahili civilization (Nakamura, 2012). However, there is little understanding of the intricate relationship between the environment and human activities in the vicinity of important settlements such as Songo Mnara. Songo Mnara Island, located in Tanzania, is a Stonetown along the East African coast (Wynne-Jones and Fleisher, 2015). This site has archaeological significance as a well-preserved exemplar of the Swahili tradition. It dates to the 14th and 15th centuries, which was the peak of the Swahili trading civilization, and together with neighbouring Kilwa was one of the richest and most prominent towns on the coast (Fleisher, 2014; Sulas et al., 2019; Wynne-Jones and Fleisher, 2015). This study provides insights into long-term vegetation dynamics and climate change, including sea-level fluctuations and societal interactions and adaptations, in an area where the sea and climate profoundly influenced human existence and resource availability and possible human responses to different episodes of these changes.

Palaeoenvironmental data based on a single proxy can be limiting; by combining multiple proxies we can improve the interpretive power of the results. While previous studies have been conducted on geophysical and geochemical analyses, artefact distribution, and anthropogenic modifications of the coastline of Songo Mnara (Fleisher, 2014; Fleisher and Sulas, 2015; Pollard et al., 2012), there is no palynological work that combines insights on mangrove dynamics and links environmental archives from sediment cores and archaeological soil samples. This study presents the first attempt to investigate the palaeoenvironment using multi-proxy analysis of both mangrove sediment and soil samples collected from archaeological context (Fig. 1). To obtain an extensive and detailed record of environmental changes, this study employed multiple proxies including pollen analysis to indicate vegetation dynamics and sea-level fluctuations (Cohen et al., 2021; Mustaphi et al., 2021; Punwong et al., 2013a). Phytolith analysis is used to infer human activities during the domestication of crop plants such as maize and millet (Gao et al., 2023; Piperno et al., 2009). Charcoal analysis is used to investigate past fire regimes and human activity (Ma et al., 2020; Whitlock and Larsen, 2001), whereas particle size and loss-on-ignition analyses provided supplementary evidence of hydrological regime and sea-level changes (Sanders et al., 2012; Wang et al., 2023). Furthermore, geochemical analysis corroborated the palaeoclimatic conditions and human influence in the area (Castañeda-Posadas et al., 2022; Tchounwou et al., 2012; Wang et al., 2023). The integration of these data with carbon-14 dating enables the investigation of the developmental patterns and vegetation dynamics of mangrove ecosystems, which can then be used to infer the impact of past environmental changes on the ecosystem. This approach provides insights into the potential connections between settlement, development, and abandonment in Songo Mnara, Tanzania. To provide a broader view, the findings of this study will be integrated with previous research to the regional-scale dynamics along the Swahili coast of East Africa.

1.1. Regional setting

Songo Mnara Island is a nearshore island in the Kilwa archipelago on the southern coast of Tanzania, 200 km from Mozambique's border (Pollard et al., 2012; Sulas and Madella, 2012) (Fig. 2). The island is connected to the Sanje ya Majoma Islands by mangrove forests and is divided from Kilwa Kisiwani, which is also a part of the Kilwa region, by a 3 km wide channel (Pollard et al., 2012). Climate and rainfall are influenced by the northeast and southern monsoon systems, which are controlled by the Intertropical Convergence Zone (ITCZ) (McClanahan, 1988). The northeast monsoon occurs between November and March, whereas the southern monsoon is active from May to June. The rainfall amount of Songo Mnara is similar to the central and southern mainland of Tanzania around 1000–1800 mm year^{-1} (Indeje et al., 2000; McClanahan, 1988; McParland, 2017). The geology of the Kilwa region consists of bedrock of upper Cretaceous to lower Miocene clay stones with limestone and sandstone (Nicholas et al., 2007). Songo Mnara is situated on the East African coral reef (Adojoh et al., 2023; Ruiz-Fernández et al., 2018) and is typically composed of limestone areas, natural quartz sand, and sandy clay deposits. The coral bedrock is covered with shallow subsoil of degraded coral sands (Nicholas et al., 2007; Stoetzel, 2014). The northern, northeastern, and southern edges of Songo Mnara are close to those of mangrove forests (McParland, 2017; Pollard et al., 2012). There are six dominant mangrove species at the Songo Mnara (Stoetzel, 2014), namely *Avicenia marina, Bruguiera gymnorrhiza, Ceriops tagal, Rhizophora mucronata, Sonneratia alba*, and *Xylocarpus granatum*. In addition to mangrove forests, a diverse range of vegetation types exist on this island, including coastal dry forests, impenetrable mixed scrub forests, maritime scrub forests, *Brachystegia* forests, riverine forests, and freshwater swamp forests (Stoetzel, 2014). Moreover, there is a large plantation of *Cocos nucifera* at Songo Mnara, and baobab trees (*Adansonia digitata*) are also found near the ruins of Songo Mnara (McParland, 2017). Crops, including *Sorghum bicolor*, *Pennisetum glaucum*, and *Carica papaya*, are observed in close proximity to Songo Mnara within the village of Mikadi, located approximately 1.5–2 km away from the archaeological site (McParland, 2017).

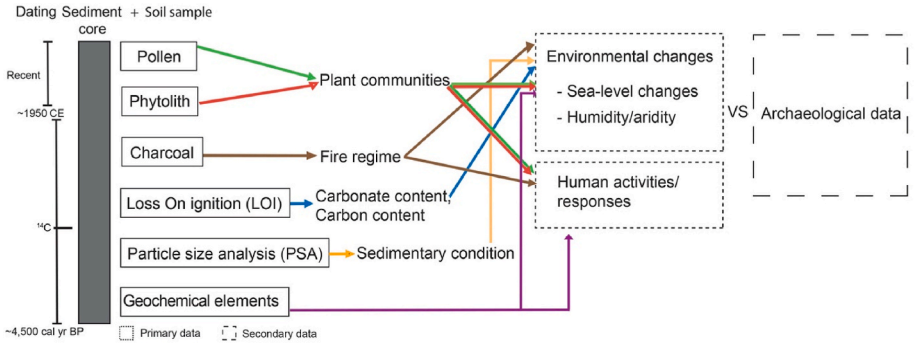

Fig. 1. Summary of proxies for inferring environmental changes and human activities in this study.

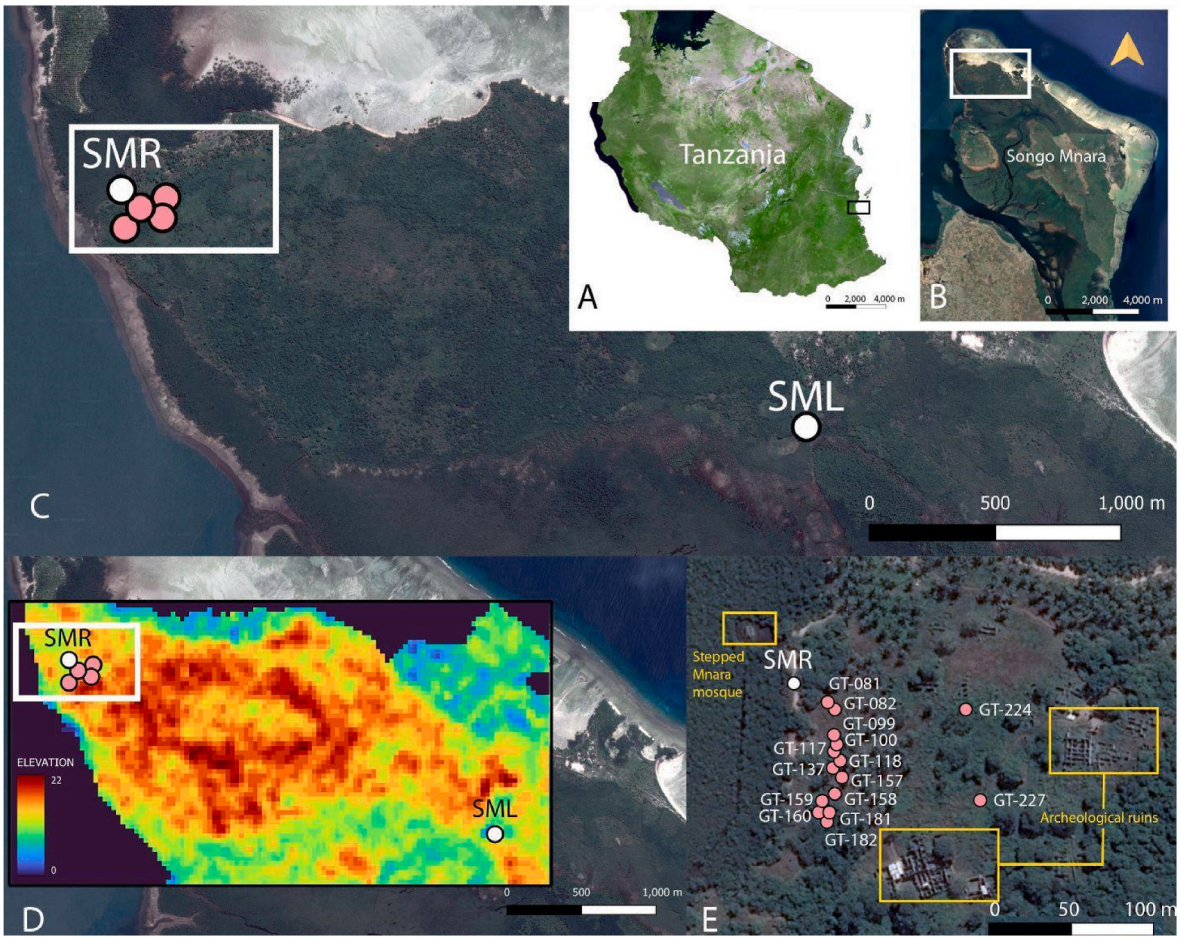

Fig. 2. Study site. (A) The site is within a black rectangle in the map of Tanzania (GISGeography, 2023); (B) core and soil collections were made in an area covered by a white rectangle in the map of Songo Mnara (Google, 2022); (C) coring sites (white circles) and soil pits of archaeological area (pink circles) on the right and left sides of the island (SMR and SML, respectively); (D) digital elevation model (DEM) map of Songo Mnara providing an approximate altitudinal heights in meters for the study site; (E) details in a white rectangle of (C) and locations of archaeological ruins and a stepped Mnara mosque ruin (yellow boxes) relative to cores/soil collecting sites. Elevation data in the DEM map at the sampling locations were extracted from NASA Version 3.0 SRTM (NASA JPL, 2013) using ArcGIS. The spatial resolution of the data was 1 arcsec at the equator and approximately 30 m horizontally. The absolute height error of the African data was 5.6 m (Rodriguez et al., 2006). (For interpretation of the references to colour in this figure legend, the reader is referred to the Web version of this article.)

1.2. Archaeological background

The Songo Mnara site, situated in the northwest corner of Songo Mnara Island, was founded and occupied for a relatively short period of 150 years between the late 14th and 16th centuries and was distinguished by a significant investment in architecture constructed of coral (Pollard et al., 2012; Wynne-Jones, 2013). The site was abandoned when Kilwa was partially depopulated after the arrival of the Portuguese at approximately 1500 CE (Chittick, 1974; Wynne-Jones, 2013). Songo Mnara is a one of a series of 'stonetowns' along the East Africa coast built during the 'Golden age' of Indian Ocean trade in the 14–16th centuries (Pouwels, 2002; Wynne-Jones, 2013). Stonetowns are coral-built settlements on the Swahili coast that include stonehouses, wattle and daub structures, mosques, and tombs (Stoetzel, 2014; Sulas and Madella, 2012). According to an archaeological investigation, the site contains three enclosed open spaces, six mosques, four cemeteries, and two dozen housing blocks (Fleisher and Wynne-Jones, 2012). The variety of house styles at the site suggests that they were occupied by a diverse group of people. Elite members would have organised the town's management and planning, as seen by the significant grand architectural style of the most elaborate settlement structures, such as mosques and the town wall. Small coral houses at this site reveal a different class of families involved in both local and global economies, as indicated by the discovery of imported ceramics and locally minted coins, even among the smallest coral buildings (Fleisher, 2014). Songo Mnara was reoccupied in the middle to late 19th century but not at an ancient site (Wynne--Jones and Fleisher, 2015). A modern village is situated on the eastern coast of the island, about a 30-min walk from the archaeological site, which is bordered by irrigated rice fields on the southern part of the island (Wynne-Jones and Fleisher, 2015).

2. Materials and methods

2.1. The field methods and collection

The vegetation on Songo Mnara Island was surveyed in April 2022, and the ecological distribution and dominant mangrove species along the coast were recorded. Sediment cores were taken from mangrove areas at Songo Mnara during the field survey using a Russian-type corer (5-cm diameter x 50-cm length). Survey cores were conducted and ranged in depth from 30 cm to a maximum of 120 cm due to impenetrable coral-bed rock. Therefore, only two cores of 80 cm SMR (9.039076S, 39.550582E) and 120 cm SML (9.049167S, 39.576074E) were collected from two different mangrove locations (Fig. 2). The core SMR is landward of small mangrove areas approximately 300 m from the sea in the northwest of the island. The core SML is also landward, but of a larger mangrove area to the northeast of the island, 3 km away from SMR. The mangroves surrounding the SML were connected to the sea by

a tidal creek located approximately 2.3 km away at the shortest distance from the open sea. The other edge of the mangroves in the SML was connected to the adjacent grassland areas (Fig. 3E). The sediments were transferred to PVC pipes and wrapped in aluminum foil for transportation to cold storage in the Department of Environment and Geography, University of York. Seventeen soil samples of three landscape types were obtained using a Shovel Test Pit survey (STPs) from the cultural layer from 8 to 56 cm in the open areas (Fig. 2E) as part of the Songo Mnara Urban Landscape Project. These soil samples were situated close to the mangrove area and core SMR. The samples were kept in plastic bags and stored in the cold storage at BioArCh at the University of York.

2.2. Chronology

The chronology of the cores was established based on accelerator mass spectroscopy (AMS) radiocarbon dates of two charcoal/bark and three bulk sediments from the DirectAMS Radiocarbon Dating Service, USA. The samples were selected from the basal sections and places of biostratigraphic changes in mangrove cores. Two samples were treated with acid-base-acid (ABA) method following Brock et al. (2010) to remove soluble carbonates and prevent humic acids from percolating into the mangrove sediment sequences. Age-depth models were produced using the package 'rBacon' in the R statistical programming language version 3.4.0 (Blaauw and Christen, 2013; R Development Core Team, 2017). In this study, the surface sample collected at 0 cm depth serves as a reference point for the present year, which is 2022 CE. Calibration was performed using a Southern Hemisphere calibration curve (SHCal20) that provided a range with 95% confidence intervals (Hogg et al., 2020). All calibrated dates within this work are presented as calibrated years before the present (cal yr BP), BCE (Before Common Era) and CE (Common Era).

For the soil samples, chronology was obtained from previous archaeological research at this site (Fleisher, 2014; Fleisher and Sulas, 2015). Although the exact dates for the soil samples were not available, they were recorded based on the cultural materials found within each cultural layer.

2.3. Pollen, phytolith and charcoal analyses

Sediment samples were sub-sampled at 2 cm intervals along the cores SMR and SML for pollen, phytolith, and charcoal analyses. Two grams of

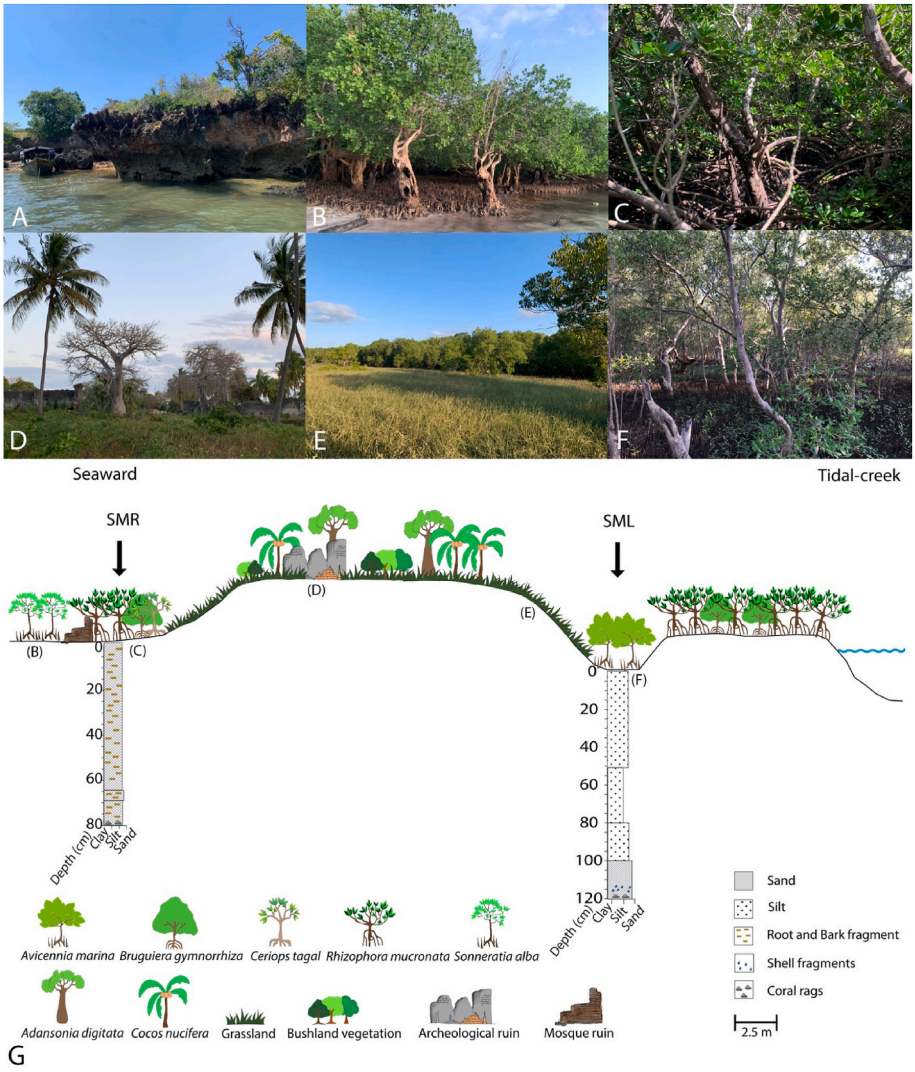

Fig. 3. Vegetation in the study site from the seaward area of the SMR to SML coring sites: (A) limestone cliff exposed to the sea with grassland/scrub; (B) seaward area dominated by *Sonneratia alba*; (C) the SMR coring site covered with *Rhizophora mucronata*; (D) archaeological ruin with coconut trees and baobabs; (E) grassland adjacent to the mangrove in SML; (F) the SML coring site with extensive pneumatophores of *A. marina*; (G) a schematic representation illustrating the ecological distribution and dominant species in the mangrove area, coring site, and archaeological ruin of Songo Mnara based on the DEM, with detailed information about the stratigraphy of the SMR and SML cores.

each soil sample were subjected to pollen, phytolith, and micro-charcoal analyses. One hundred wet-sediment samples (1 cm^3) and seven soil samples were extracted for pollen analysis. Pollen preparation was performed following standard procedures, including acetolysis (Erdtman, 1969; Faegri and Iversen, 1989) and heavy liquid separation with a sodiumpolytunstate solution (Hunt et al., 1985). To estimate pollen concentration, *Lycopodium* spores were added to each sample (Bonny, 1972; Smol et al., 2001). Pollen identification was performed using modern pollen references (Chumchim, 2010; Punwong, 2008) and compared with pollen from mangrove specimens collected during fieldwork. To estimate the optimal grain count the number of pollen taxa in five samples from each coring site were counted and recorded for every 20 grains, up to a count of 200 grains. After 80 grains no new taxa were discovered; as a result 150 pollen grains were calculated as percentages and are presented as pollen diagrams. However, pollen is frequently poorly preserved in soil samples from archaeological sites; consequently, relatively few pollen grains are extracted from these soil samples. Constrained incremental sums of squares cluster analysis (CONISS) was used to statistically determine zonation within the TILIA2 and TILIA*Graph software (Grimm, 1991). Pollen data were classified into mangrove, back mangrove, terrestrial herbaceous, non-mangrove arboreal, and unknown groups. Mangroves and back mangroves were categorized according to Watson's (1928) and Santisuk's (1983) inundation classes. Pteridophyte spores were excluded from the pollen sum.

Phytoliths were also extracted from 1 cm^3 of wet-sediment and 2 g of soil samples according to Madella et al. (1998) using a combination of pre-treatment methods to remove sand, clay, and organic material from the samples and gravity sedimentation with flotation in a heavy liquid with a specific gravity of 2.3 g/cm^3. The sample residues were mounted on microscope slides using a mounting medium. However, the phytolith concentration in mangrove sediments was extremely low and insufficient for analysis. Therefore, only the phytoliths from each soil sample were investigated. The extracted phytoliths were counted and described according to the International Code for Phytolith Nomenclature 2.0 (International Committee for Phytolith Taxonomy (ICPT) et al., 2019). Phytolith taxonomic identification was performed by comparison with published references (Barboni and Bremond, 2009; Mercader et al., 2009; Runge, 1999) and additional studies on similar geographic or contextual case studies (Harvey and Fuller, 2005a; Novello and Barboni, 2015; Sulas et al., 2019). At least 300 phytoliths, if the concentration allowed, with taxonomic significance, were counted per sample and categorized into four major groups according to their taxonomic origins (Sulas and Madella, 2012): Poaceae (grasses) including three sup-groups (Panicoideae, Pooideae, and undifferentiated grasses, Arecaceae, woody/herbs, and others). The phytoliths were interpreted by calculating percentages based on the total phytolith sum and are presented in a diagram within the graphics software TILIA2 and TILIA*Graph (Grimm, 1991).

Microscopic charcoal is typically identifiable by fragments that are angular in shape, opaque, and black in colour (Waddington, 1969; Patterson III et al., 1987; Pitkanen and Huttunen, 1999; Clark, 1982, 1988a, 1988b; Clark et al., 1989). However, particles less than 3 μm could be mistaken for pyrite, biotite, or marcasite (Blackford, 2000; Rhodes, 1998), and the darkening or blackening of unburned plant pieces may occur due to techniques involved in the pollen and phytolith slide process, particularly acetolysis. Therefore, they were excluded from the studycounting. The microscopic charcoal in pollen and phytolith slides were presented using size classes of microscopic charcoal adapted from Tinner and Hu (2003) and Rucina et al. (2009). Charcoal is divided into seven classes (3–10 μm, 11–25 μm, 26–50 μm, 51–75 μm, 76–100 μm, 101–149 and > 150 μm). The size of charcoal fragments can be used to infer the relative distance from the ignition source. Smaller fragments (3–100 μm) are typically associated with distant regional fires, as they can be transported over larger areas. Larger fragments (>100 μm) tend to be found closer to the fire source, suggesting a local origin and potentially establishing connections between human activities and environmental changes, especially those related to fires set by humans (Punwong et al., 2018b; Whitlock and Larsen, 2001). Charcoal counts for each size class were determined as the total number of fragments counted within a complete pollen and phytolith slide in 500 fields of 400 × magnification view (Rucina et al., 2009). The total charcoal accumulation is determined by summing the multiples of mean length, measured in millimetres (mm), and the number of fragments per calculated area for each size class on sample slides (Punwong et al., 2018b).

2.4. Stratigraphy, particle size, LOI and geochemical analyses

Sediment samples of 1 cm^3 were subsampled at 2 cm intervals along the cores SMR and SML for particle size, loss on ignition, geochemical analyses. Two grams of each soil sample were subjected to geochemical analyses.

The lithology of the sediment cores and the soil samples were described as follows: depth, colour, texture by eye evaluation and finger-texturing on dry and wet samples following a modified version of the Tro; els-Smith (1955) classification (Kershaw, 1997). Munsell soil colour charts were used to determine the colours of the sediment cores and soil samples (Color, 2009).

To determine the grain-size distribution, 100 wet-sediment samples were pre-treated with 10% HCl and 30% H_2O_2 to remove organic material and carbonates, respectively. The grain size distribution of the remaining samples was measured using a Malvern Mastersizer 2000 analyser at the University of York, with a measurement range of 0.02–2000 μm. The end-member modeling algorithm of Weltje (1997) was used to calculate the end members from the total set of grain size measurements of the cores.

Loss on ignition (LOI) procedure was performed as described by Heiri et al. (2001). Organic matter and carbonate contents of each wet-sediment sample were determined by weight loss on ignition (LOI) at 550 °C and 950 °C respectively (Heiri et al., 2001).

Geochemical analysis was conducted using a handheld X-ray fluorescence analyser at the Department of Geology, Faculty of Science, Chulalongkorn University. A total of 100 dry-sediment samples and 17 soil samples were analysed in extra-soil mode using a large-area silicon-drift detector, with a 3 × 60 s acquisition time (beam) at accelerating voltages ranging from 8 to 40 kV. The resulting XRF powder data provide concentrations in parts per million (ppm) for various elements, including phosphorus (P), sulfur (S), potassium (K), calcium (Ca), titanium (Ti), magnesium (Mg), iron (Fe), nickel (Ni), zinc (Zn), strontium (Sr), zirconium (Zr), and lead (Pb). Furthermore, the concentrations of Ti, Zr, Fe, and S were selected to compute the Ti/Zr and Fe/S ratios, which offer valuable insights into sedimentary environments. Ti and Fe contents potentially suggest the presence of terrigenous sediments, whereas the Zr contents are associated with coastal placer formation (Bahr et al., 2005; Ma et al., 2020; Nace et al., 2014; Rozan et al., 2002). Therefore, a high Ti/Zr concentration suggests that the sediments originated predominantly from terrestrial sources (Adojoh et al., 2023; Ruiz-Fernández et al., 2018). Conversely, a pronounced representation of Fe/S indicates the presence of marine shale deposited on the continental shelf, which is associated with an anoxic period characterised by heightened concentrations of Fe and sulfur (pyrite) within the sediment (Doktorgrades, 2004; Kakroodi et al., 2012; Mendoza, 2007; Zabel et al., 2001).

3. Results

3.1. Vegetation survey and mangrove zonation in Songo Mnara, Tanzania

The vegetation and mangrove forests on Songo Mnara Island were surveyed (Fig. 3A–F). The ecological distribution and dominant mangrove species are presented in this study (Fig. 3G). The position and environmental gradients of each mangrove species found in this study

are similar to mangrove zonation in Tanzania as recorded by Punwong et al. (2013c). *S. alba* and *R. mucronata* dominated the seaward area. The core SMR is dominated by *R. mucronata* (70%), *C. tagal* (20%), and *B. gymnorrhiza* (10%) trees. The core SML was characterised only by *A. marina* (100%). According to DEM data, the core SMR is higher than the core SML.

3.2. Chronology

Five radiocarbon dates were obtained from cores SMR and SML as shown in Table 1. Since the radiocarbon dating at the basal part of core SML was 518 cal year BP, getting close to the limit of C^{14} dating (Nichols, 2009), the dating of the overlaying layer possibly provides the modern age (after 1950 CE). Therefore, the chronology of core SML was determined by interpolation between a single dated sample at 78 cm and the top of the sediment sequence, which was 2022 CE, i.e when the core was collected. The homogeneous sediment and insignificant change in biostratigraphy allow us to assume further the continued deposition of 1.3 mm $year^{-1}$, which is comparable with that obtained from other mangrove sediments in the Indian Ocean during the past 500 years, i.e., 0.8–1.6 mm $year^{-1}$ in Unguja Ukuu, Zanzibar, Tanzania (Englong et al., 2023), ~1.4 mm $year^{-1}$ in Mahé, Seychelles (Woodroffe et al., 2015), and 0.6–1.78 mm $year^{-1}$ in Kon Kan (Limaye and Kumaran, 2012) in coastal India. The consistency in the sedimentation rate of the mangrove environment across the Indian Ocean strengthens our treatment of the chronology for core SML. The median date was used to report ^{14}C dates in this study, and the max-min date range was presented as a calibrated year before the common era (BCE) and the common era (CE) following the Gregorian calendar. The age-depth models for both mangrove sediment cores are presented in Fig. 4. Accordingly, it revealed that the deposition of organic deposits in the cores SMR and SML started around 1432 CE and 2592 BCE, respectively. Dating of all soil samples from Songo Mnara were previously determined by Fleisher (2014) and Fleisher and Sulas (2015) to range from the late 14th to early 16th centuries CE.

3.3. Pollen records

Pollen was not extracted in sufficient amounts from soil samples, likely due to high oxygen exposure, resulting in decay and decomposition of pollen grains (Havinga, 1967). However, a few domesticated grass pollen grains were found under a light microscope in some samples. Domesticated grass pollen were recognised by a grain diameter and annulus size larger than 40 μm and 8.5 μm, respectively (Hapsari and Ballauff, 2022; Joly et al., 2007; Quamar and Kar, 2022). These findings were presented along with other results in soil samples. In contrast, pollen grains were well preserved in the sediment cores due to anoxic conditions, and the extraction yield was much better, as presented in a stratigraphic diagram and described as follows.

3.3.1. Pollen diagram description of the core SMR

The pollen diagram of core SMR was separated into three zones: SMR-1 (80-52 cm; 1430–1630 CE), SMR-2 (52-22 cm; 1630–1870 CE), and SMR-3 (22-0 cm; 1870 – present day), as shown in Fig. 5A.

SMR-1 (80-52 cm; 1430–1630 CE): Mangroves had the highest appearance (73–92%), followed by terrestrial herbaceous species (4–20%), and non-mangrove arboreal species (3–10%). Mangroves were present with *R. mucronata* (68–80%), *Bruguiera/Ceriops* (0–11%), *S. alba* (0–7%), and *A. marina* (0–1%). Terrestrial herbaceous species were characterised by Poaceae (4–20%) and Cyperaceae (0–2%). Non-mangrove arboreal species represented low percentage values with Anacardiaceae (0–3%), Convolvulaceae (0–3%), Fagaceae (1–5%) and Myrtaceae (0–2%). The pollen concentrations varied between 4,194 and 22,665 grains/cm^3.

SMR-2 (52-22 cm; 1630–1870 CE): Mangroves characterised by *R. mucronata* (52–80%) and *S. alba* (0–2%) gradually decreased while *Bruguiera/Ceriops* (3–12%) and terrestrial herbaceous species including Asteraceae (0–2%), Cyperaceae (0–3%) and Poaceae (7–29%) increased. Non-mangrove arboreal species were present at low percentages. Pollen concentrations varied between 7562 and 15,512 grains/cm^3.

SMR-3 (22-0 cm; 1870 – the present day): Mangroves were the primary group (80–90%), dominated by *R. mucronata* (49–84%) and *Bruguiera/Ceriops* (4–21%). The abundance of *S. alba* (0–1.4%) increased at the top. Terrestrial herbaceous species (7–16%), characterised by Poaceae (6–15%) and Asteraceae (0–0.7%), decreased slightly from the previous zone. Non-mangrove arboreal taxa (0–5%) were rare with Anacardiaceae (0–3%), Convolvulaceae (0–0.8%), and Fagaceae (0–4%). Pollen representation ranged from 4,159 to 11,018 grains/cm^3.

3.3.2. Pollen diagram description of the core SML

The pollen diagram of the core SML was divided into five zones: SML-1 (120-72 cm; 2590 BCE – 490 CE), SML-2 (72-52 cm; 490–1430 CE), SML-3 (52-24 cm; 1430–1760 CE), SML-4 (24-14 cm; 1760–1870 CE), and SML-5 (14-0 cm; 1870 CE– present day), as shown in Fig. 5B.

SML-1 (120-72 cm; 2590 BCE – 490 CE): Mangroves were most common (92–98%), followed by back mangroves (0–3%), non-mangrove arboreal species (2–8%), terrestrial herbaceous species (0–1.3%) and unknown pollen (0–3%). Mangroves were characterised by *R. mucronata* (52–83%), *S. alba* (0–17%), *Bruguiera/Ceriops* (1–21%), and *A. marina* (4–38%), and back mangroves were dominated by *Lumnitzera* (0–3%). Non-mangrove arboreal species (2–8%) were recorded at low percentages. The percentage of terrestrial herbaceous species was very low. Pollen concentrations varied between 5,990–28,429 grains/cm^3.

SML-2 (72-52 cm; 490–1430 CE): Mangroves remain the most common (53–97%), characterised by *R. mucronata* (27–76%) and *Bruguiera/Ceriops* (15–27%). The back mangroves had almost disappeared. A low percentage of non-mangrove arboreal areas was present. Terrestrial herbaceous species increased toward the top (0–27%). The pollen concentrations fluctuate and ranged from 5111 to 28,439 grains/cm^3.

Table 1
Radiocarbon dates of sediment cores from Songo Mnara mangroves. Dates were calibrated using a Southern Hemisphere calibration curve (SHCal20) (Hogg et al., 2020).

Core	Depth (cm)	Code	Sample type	^{14}C yr BP	Min-max date range (Cal yr BP)	Median date (Years BCE/CE)	Median date (Cal yr BP)	Sedimentation rates (mm yr^{-1})
SMR	78	D-AMS 047715	Charcoal, bark	521 ± 27	477–615	1432 CE	518	1.32 (0–78 cm)
SML	42	D-AMS 051617	Bulk sediment	346 ± 23	313–473	1544 CE	406	0.88 (0–42 cm)
	58	D-AMS 049617	Bulk sediment	665 ± 24	550–660	1329 CE	621	0.77 (42–58 cm)
	82	D-AMS 051618	Bulk sediment	2198 ± 25	2009–2303	185 BCE	2135	0.16 (58–82 cm)
	118	D-AMS 047717	Charcoal, bark	4106 ± 28	4373–4784	2592 BCE	4542	0.15 (82–118 cm)

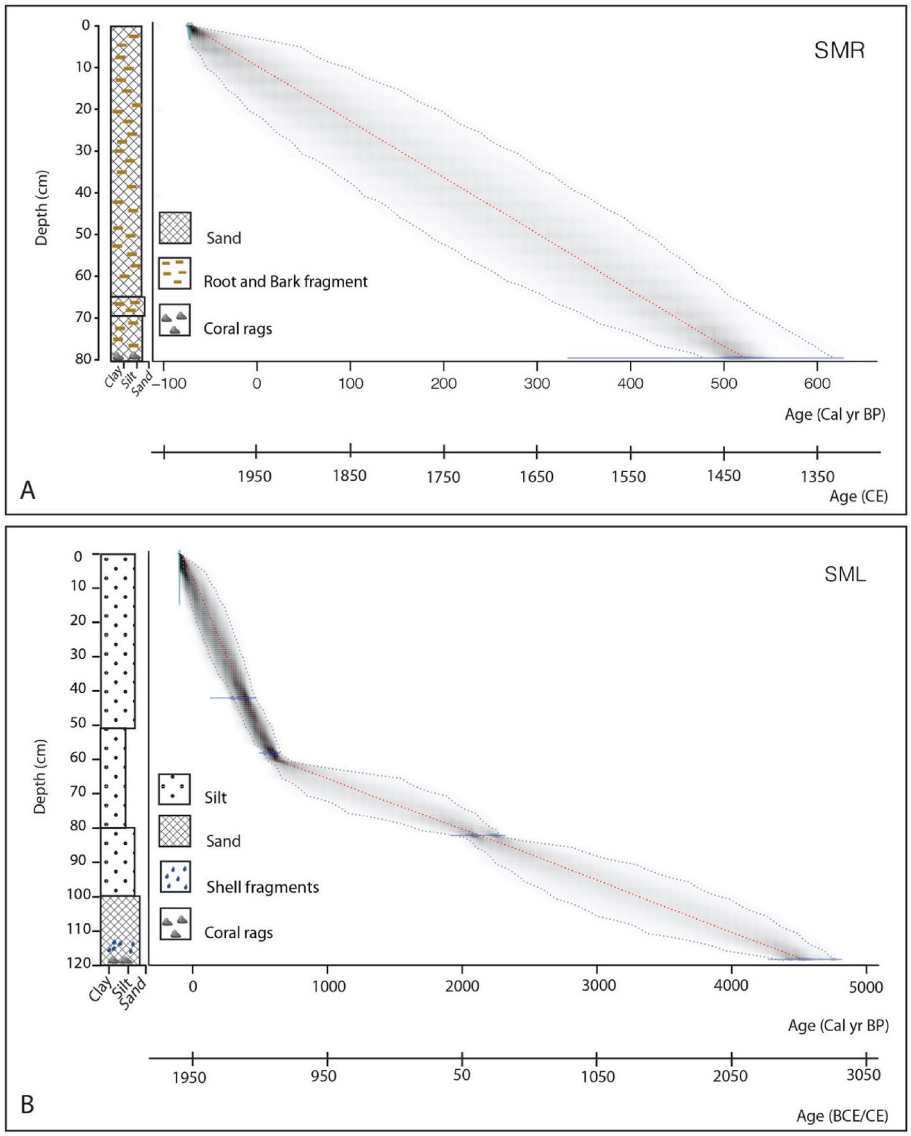

Fig. 4. Age-depth models of cores SMR (A) and SML (B).

SML-3 (52-24 cm; 1430–1760 CE): Mangroves, particularly *R. mucronata* (27–70%), declined at the beginning and increased at the top. No back mangroves were present in this zone. Non-mangrove arboreal taxa (3–8%) were rare, with only Fagaceae. Terrestrial herbaceous species suddenly increased significantly along with Poaceae and Cyperaceae. Pollen concentrations ranged from 567 to 19,650 grains/cm^3.

SML-4 (24-14 cm; 1760–1870 CE): Terrestrial herbaceous species (50–81%) were dominated by Poaceae (17–77%). Mangroves suddenly decreased with *R. mucronata* (0–50%). However, *S. alba* (0–20%) increased at the top. No back mangroves presented in this zone. The number of non-mangrove species increased with *Podocarpus* sp. (0–20%). Pollen concentrations fluctuate and ranged from 10,552 to 21,406 grains/cm^3.

SML-5 (14-0 cm; 1870 CE – the present day): Mangroves sharply increased again, characterised by *R. mucronata* (17–44%), *Bruguiera/Ceriops* (8–17%), and *A. marina* (18–52%). Terrestrial herbaceous species (13–23%) with Poaceae and Cyperaceae sharply decreased. The abundance of non-mangrove arboreal species (0–3%) with *Podocarpus* sharply decreased. Pollen concentrations varied between 3,046–23,393 grains/cm^3.

3.4. Phytolith records

Seventeen soil samples collected from open areas close to mangrove forests yielded various types and amounts of phytoliths shown in the phytolith diagram (Fig. 6), where sixteen morphotypes were identified and categorized. The detailed phytolith descriptions are provided following the phytolith diagram in each landscape type.

Coastal ridge (GT-81-GT-210): Undifferentiated grasses dominated the phytolith morphotypes (27–66%), including elongate dentate (0–7%), elongate entire (11–54%), elongate sinuate (0–26%), bulliform flabellate (1–22%), and rondel (0–3%) morphotypes. The woody morphotype (14–52%) comprised blocky (11–43%) and tracheary annulate (0–7%) forms, whereas the spheroid echinate (0–28%) belongs to Arecaceae. The remaining phytolith morphotypes fell into three categories: Panicoideae (0–8%), Pooideae (0–5%), and other groups (2–29%), but they were present in small percentages of all samples. Notably, the GT-210 sample stood out with a significant representation of the cross morphotype from the Panicoideae group, accounting for 3% of its composition.

Inland forest patch (GT-224): Undifferentiated grasses (45%) were the dominant morphotypes, although elongate (9%) was notably lower than the coastal ridge landscape. The woody morphotypes (45%),

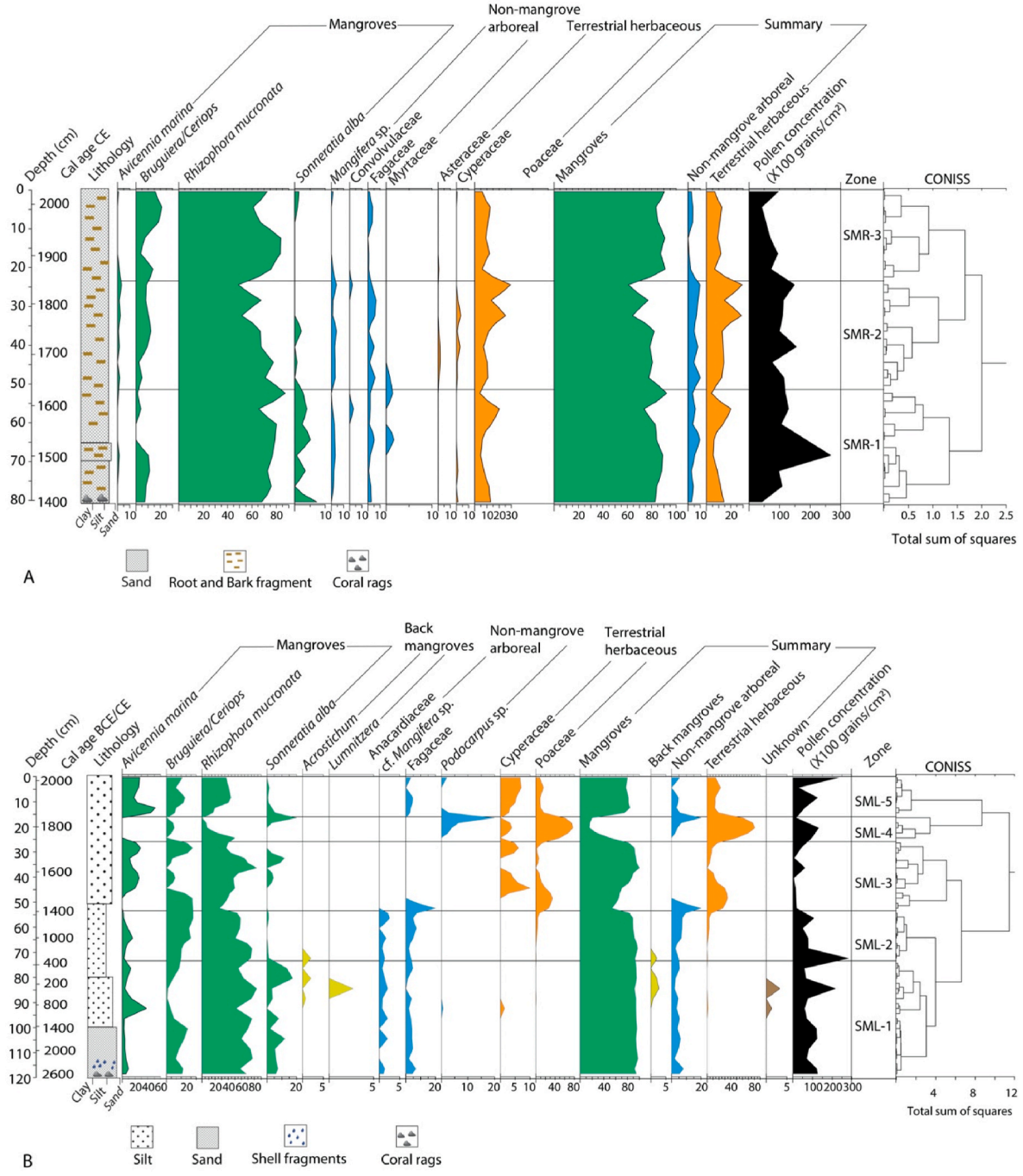

Fig. 5. Pollen diagram of the cores SMR (A) and SML (B) showing pollen percentage of plant taxa. The Y-axis represents dating calculated by the age-depth model using rBacon.

particularly blocky (44%), also had a significant representation in this area. The cross morphotype (2%) of the Panicoideae group was still present in this landscape. Additionally, other morphotype groups, namely Arecaceae, Pooideae, and others, were also present, but at low percentages.

Coconut field close to archaeological ruin (GT-227): Undifferentiated grass morphotypes (84%) including elongate entire (80%), and bulliform flabellate (4%) had the highest representation when compared to other landscapes. Woody morphotype (11%), including blocky, was dramatically lower than that of the inland forest patch. Cross morphotype (1%) of the Panicoideae group was lowest among all landscape types. Pooideae, Arecaceae and other morphotypes are not present in this landscape.

3.5. Micro-charcoal records

Following the pollen zone in the pollen diagrams, charcoal fragments in each size class and the total charcoal content of the two sediment cores are shown (Fig. 7A and B).

The maximum value of charcoal accumulation in the core SMR was recorded at approximately 99 fragments/mm^2 at a depth of 24 cm (~1850 CE), and the minimum value was recorded at 8 cm (~1970 CE) at approximately 12 fragments/mm^2. The charcoal abundance in the SMR-1 zone was relatively high, ranging from 17 to 83 fragments/mm^2. Between 54 and 58 cm (~1580–1610 CE), two larger fragment classes (100–149 μm and >150 μm) appeared. Charcoal accumulation in the SML-2 zone fluctuated and declined, although the size class of the

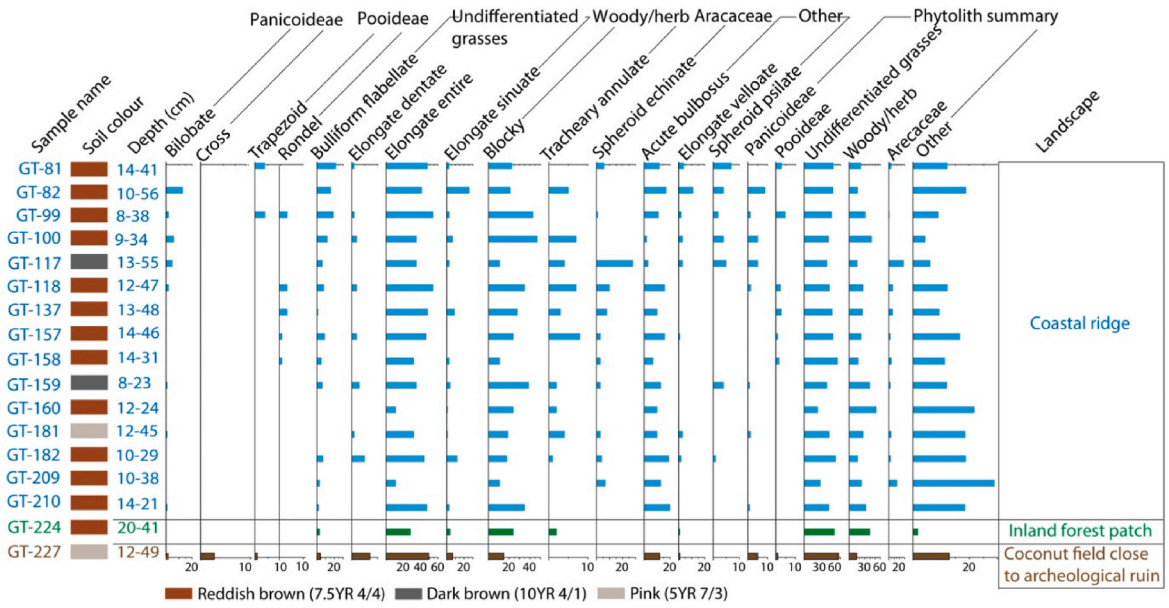

Fig. 6. Phytolith diagram of soil samples from Songo Mnara.

100–149 μm charcoal fragments increased. The total accumulation of charcoal significantly decreased in the SMR-3 zone, with decreases in all size classes, except for the notable peak of the largest particles at 4 cm.

Core SML had the highest charcoal abundance in the SML-1 zone, ranging from 11 to 71 fragments/mm^2. The largest charcoal fragments were present in this zone between the depths of 74–82 cm (~320 CE-180 BCE) and 98–102 cm (~1290-1540 BCE). In SML-2, 3, and 4 zones, charcoal contents in fragment size classes 76–100 μm, 101–149 μm, and >150 μm suddenly disappeared. Charcoal records of fragment sizes smaller than 75 μm increased from 14 cm to the topmost core in SML-5 zone, with some peaks of size class 101–149 μm, and charcoal accumulation was 2–45 fragments/mm^2.

The micro-charcoal records of the soil samples were characterised for three distinct landscape types, as shown in Fig. 8 and described as follows.

Coastal ridge (GT-81-GT-210): Charcoal fragments within the size ranges of 3–10 μm and 11–25 μm display higher concentrations in all samples, particularly GT-160, GT-181, and GT-182. The total charcoal accumulation in these samples ranged from 162 to 4,940 fragments/mm^{-2}, with GT-181 showing the highest accumulation. Except for GT-117, all samples contained the largest charcoal fragment size class (greater than 100 μm).

Inland forest patch (GT-224): Charcoal fragments in the size classes of 3–10 μm and 11–25 μm dominated, with concentrations of 175 and 162 fragments/mm^2, respectively. The largest charcoal fragment size class (greater than 100 μm) was also present, with a total accumulation of 507 fragments/mm^2.

Coconut field close to archaeological ruin (GT-227): The total charcoal accumulation was comparatively low, measuring 163 fragments/mm^2. Charcoal fragments in the size classes of 3–10 μm and 11–25 μm exhibit a decrease in concentration but remain dominant in this landscape. The largest charcoal fragment size class (greater than 100 μm) was still observed, with a low representation of 19 fragments/mm^2.

3.6. Sediment and soil compositions

The core SMR contained very dark-greyish brown to black silty sand with wood and bark fragments (Fig. 7A). The core SML contained gray to very dark gray silt and sand from the bottom to a depth of 70 cm (~640 CE), with shell fragments at the bottom of the core, followed by brownish yellow silt and sand at the top of the core (Fig. 7B). Coral rags were found at the bottom of both cores. A stratigraphic description of the cores SMR and SML is congruent with particle size analysis. The core SMR contained moderately sorted medium sand and poorly sorted extremely coarse silty medium sand, with sand fractions ranging from 54 to 93%, whereas the core SML mainly contained very poorly sorted very fine sandy to very coarse silt. Along the core SML, there were variations in the percentages of silt and sand particles, ranging from 39 to 80% for silt and 13–66% for sand. Clay particles were also present in the core SML, but only in smaller portions (0.5–19%).

Seventeen soil samples obtained from open areas were described as fine-sand silty loam soil (Fleisher and Sulas, 2015). Shell fragments were present in all samples, whereas glass bead fragments were found only in GT-100, 117, 118, 137, 157, 159, 160, 181, 182, 210, 224, and 227 (Fleisher and Sulas, 2015). A detailed description of the soil structure for each soil sample collected at Songo Mnara is shown in Fig. 6.

3.7. Loss on ignition analysis and geochemical analysis

Loss on ignition was used to investigate only the organic matter and carbonate contents of the sediment cores in the mangroves, and both agreed with the sediment composition. Geochemical analyses were provided for both sediment cores and soil samples. The organic content of core SMR ranged from 1% to 37 %, whereas the carbonate content ranged from 0.1% to 37% (Fig. 7A). The organic content fluctuated along the core and decreased at the bottom, which is related to the appearance of wood and bark fragments throughout the core. The carbonate content sharply increased in the deepest part of the core, reaching 37%, which was associated with the appearance of coral rags at the bottom of the core. The core SML had an organic content ranging from 2% to 16%, whereas the carbonate content ranged from 0.6% to 21% (Fig. 7B). The highest representation of carbonate content at the bottom of the core is also related to the appearance of coral rags and shell fragments at the bottom of the core, possibly indicating greater sea-level influence at the cored bed.

Ten elements namely S, K, Ca, Ti, Fe, Zn, As, Sr, Zr, and Ni were found in both cores SMR and SML, while Mn and Pb were exclusive to core SML. K, Ti, Zn, and Sr in core SMR remained stable from bottom to top, whereas Ca peaked in the depth range of 66–80 cm (~1520-1430 CE). S and Fe showed decreasing trends from bottom to top, whereas As had high levels in the depth range of 40–50 cm (~1720-1640 CE) before sharply decreasing. Zr was consistently present throughout, except in

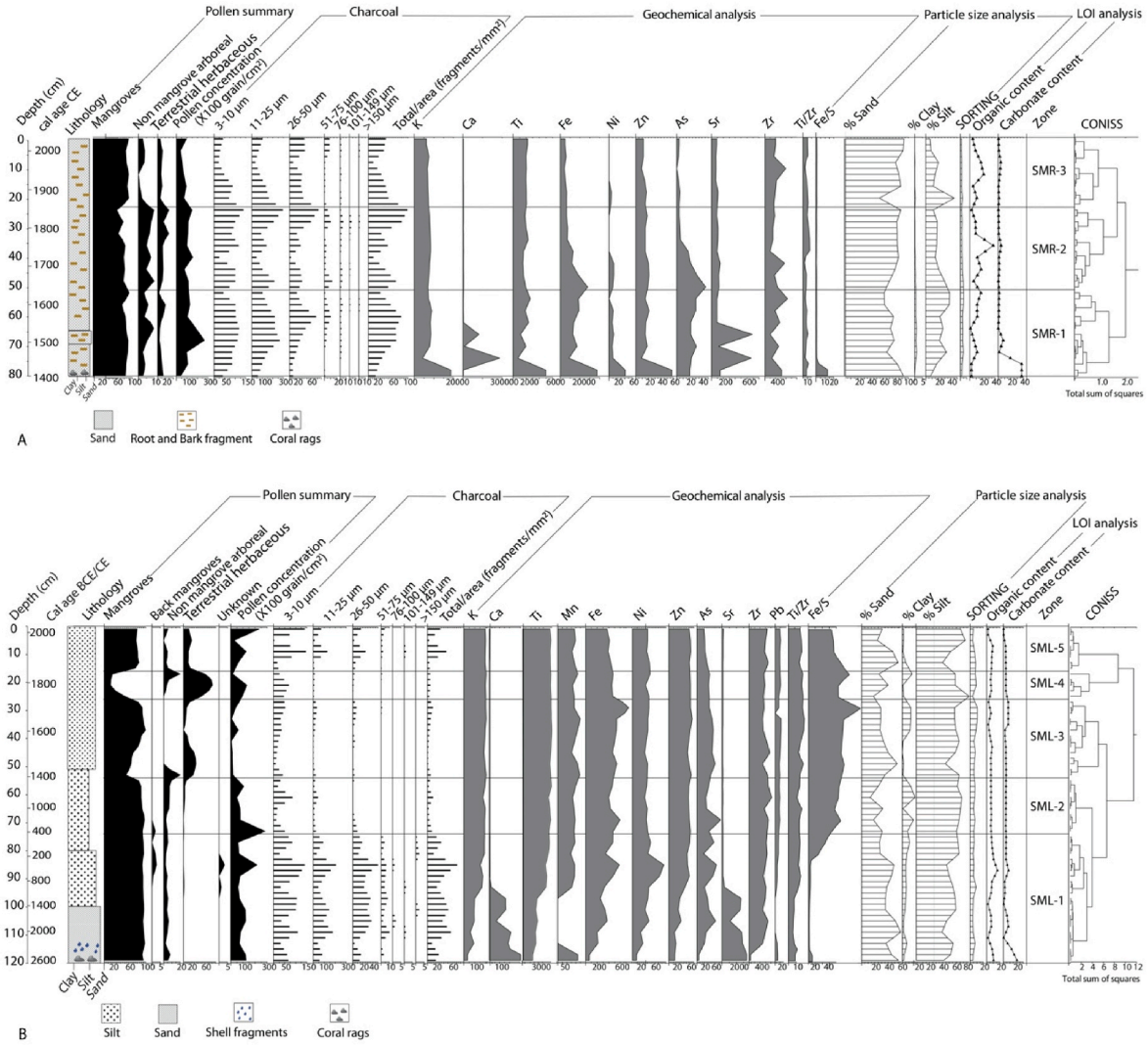

Fig. 7. Frequency plot showing pollen summary, charcoal, geochemical, particle size, and LOI data from cores SMR (A) and SML (B). Zones were based on a cluster analysis of pollen data.

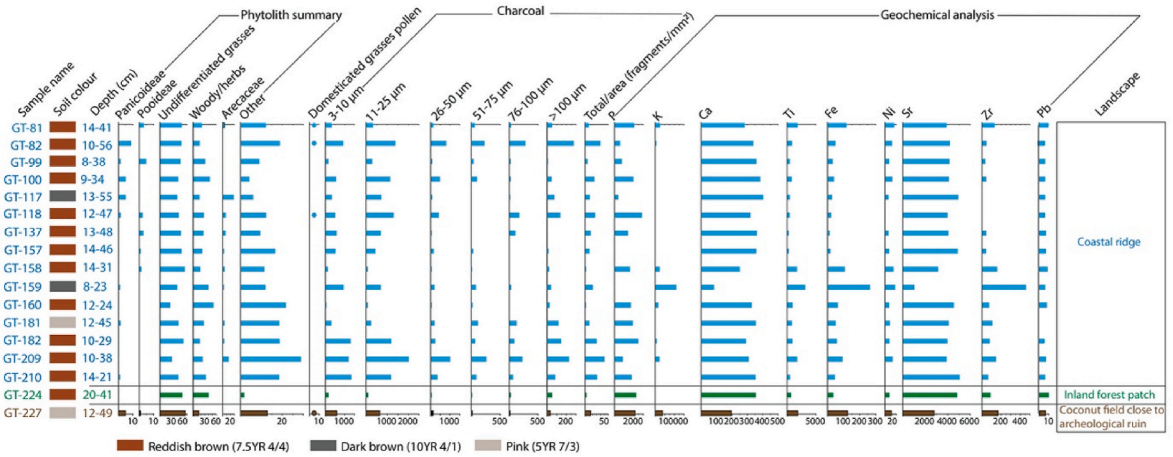

Fig. 8. Frequency plot showing phytolith summary, domesticated grass pollen, charcoal, and geochemical analysis of soil samples at Songo Mnara based on landscape types.

the deepest layer, and Ni exhibited a peak at a depth of 80 cm (~1430 CE). The Ti/Zr ratio exhibited fluctuations, with a notable increase from the middle to the top of core SMR. The Fe/S ratio demonstrated its highest representation at the bottom of core SMR, and subsequently experienced a dramatic decrease before a slight increase from a depth of 24 cm onwards (~1850 CE) (Fig. 7A). The increase in the Ti/Zr ratio, contrasted with the decrease in Fe/S ratios, possibly suggests that the bottom section was influenced by seawater rather than the upper section of the SMR core. The SML showed a similar pattern for S, K, Ti, Fe, Ni, Zn, and Zr with increasing trend from around 76–120 cm (~189 CE-2590 BCE), while Ca and Sr are represented in the depth range of 95–120 cm. Mn was stable except at 98–114 cm (~1270-2370 BCE), As fluctuated, and Pb was consistently low throughout the core. The Ti/Zr ratio sharply increased from a depth of 94 cm (~1000 BCE) to the top of the core SML, and the Fe/S ratio significantly increased from approximately 86 cm (~470 BCE) to the top, with a peak value observed between depths of 34 and 24 cm (~1760-1640 CE) (Fig. 7B). Trends in both the Ti/Zr and Fe/S ratios in the SML core also indicate that the upper section of the SML core received less influence from seawater when compared to the bottom sections. However, the peak in Fe/S possibly indicates evidence of sea-level rise in those sections.

Only nine elements were detected in the soil samples: P, K, Ca, Ti, Fe, Ni, Sr, Zr, and Pb. The results revealed that P was highly abundant in all landscape types except GT-118 and GT-157 in the coastal landscape. K was found in the coastal landscape for specific samples (GT-137, GT-157, GT-158, GT-160, GT-181, and GT-210), as well as in the inland forest patch landscape (GT-224) and coconut field landscape (GT-227). In contrast, Ca, Ti, Fe, and Sr were present in all samples, with Sr showing the highest concentration in nearly all samples. Conversely, Ni and Pb exhibited the lowest concentrations across all samples (Fig. 8).

4. Discussion and interpretation

The multi-proxy sedimentary records suggest that the mangroves in Songo Mnara were primarily shaped by relative sea-level changes and local geomorphological processes. *R. mucronata* pollen emerged as the dominant pollen type in all the sediment cores. This pollen type is primarily sourced locally, although its abundance may be exaggerated because of its wind-pollination and high pollen production (Behling et al., 2001; Ellison and Strickland, 2015). While phytoliths are abundant, especially in Poaceae, and are well-preserved under oxidizing conditions, primarily in arid environments, their diagnostic potential is limited to mangrove taxa due to low preservation rates in coastal environments (Pearsall et al., 2016; Stoetzel, 2014), where alkaline conditions prevalent often lead to their dissolution and weathering, resulting in poor preservation (Coe et al., 2017; Prentice and Webb, 2016). Therefore, in this study phytoliths retrieved only from cultural soil layers collected in dry areas provide additional insights into human activities complementing the evidence provided by pollen analysis. Based on these findings, we present and discuss the sequential records of vegetation dynamics and human-environment interaction on Songo Mnara from 2590 BCE (Figs. 9 and 10).

4.1. Environmental changes

4.1.1. Period from ~2590 to 90 BCE (4540–2040 cal yr BP)

This period started from the deepest layers of the core SML, which date to approximately 2590 BCE, coral rags are prominently present in the stratigraphy, supported by the considerable abundance of Ca and carbonate content before the SML-1 zone. The prevalence of coral rags in the bottommost layers of the core SML and the elevated presence of Ca and carbonate content can be attributed to the geomorphological history of Songo Mnara, situated on the East African coast (Arthurton, 2003; Nicholas et al., 2007). These coral reefs have evolved over an extensive period of calcium carbonate sedimentary deposition and degradation at the land-ocean boundary during the Pleistocene (Arthurton, 2003). Consequently, the significant signals, including the presence of coral rags and the high representation of Ca and carbonate contents, indicate that the area was submerged by the sea and lacked vegetation prior to 2590 BCE (Figs. 9 and 10). This observation aligns with the recorded evidence of mid-Holocene sea-level rise (5950–2650 BCE) in Tanzania (Punwong et al., 2018a) and is consistent with the mid-Holocene sea--level highstand along the southern African coastline at approximately 2850 BCE (Ramsay, 1996a,b).

In the SML-1 zone, the prevalent presence of seaward mangrove taxa, particularly *R. mucronata* and *S. alba*, suggests a potential sea level decline after 2590 BCE. This may have facilitated the establishment of mangroves on coral rags (Fig. 9), especially in areas directly affected by marine tidal water. Further sea-level lowering was observed (Fig. 10), characterised by a decrease in *R. mucronata* and *S. alba*, in contrast to an increase in *A. marina* from 1400 to 90 BCE. Although *A. marina* is typically regarded as a pioneer species inhabiting seaward edges

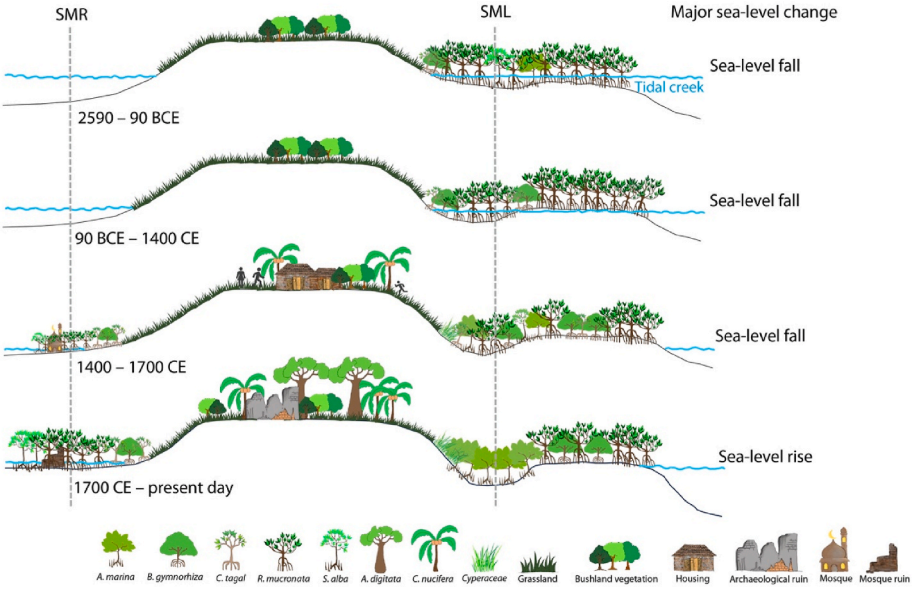

Fig. 9. Summary of major vegetation, sea-level and landform changes with human activities recorded at Songo Mnara from around 2950 BCE until the present day.

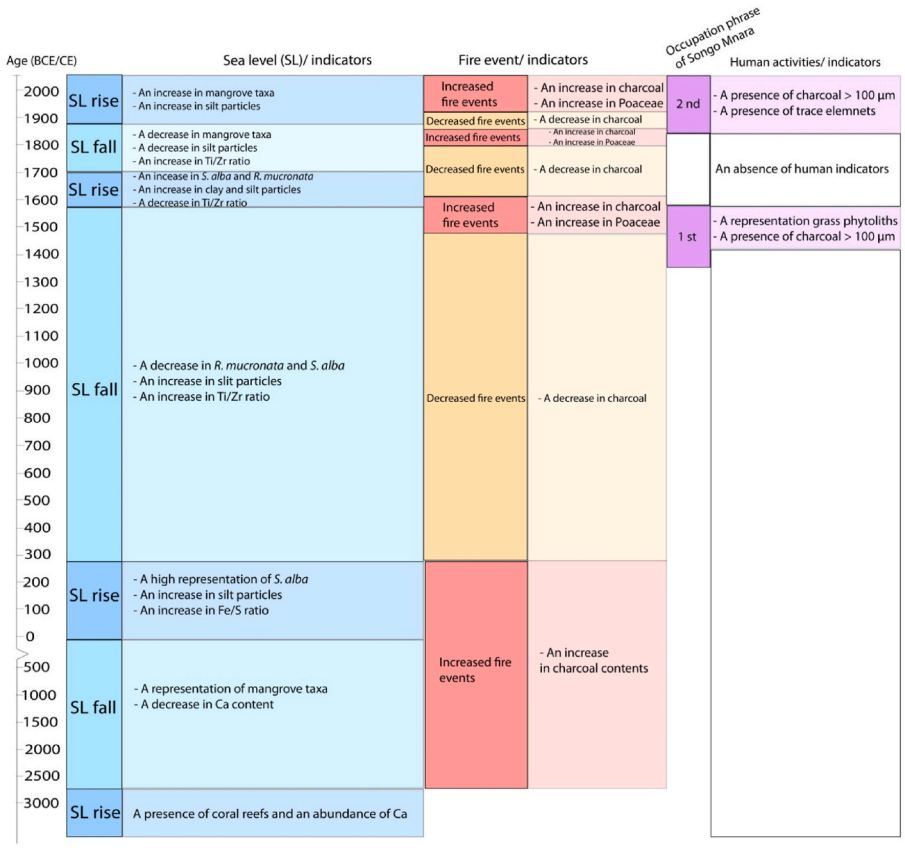

Fig. 10. A synthetic diagram illustrating the main findings of the environmental changes and the human activities in Songo Mnara, referred from palaeoecological proxies.

inundated by medium to high tides, it also exhibits a bimodal distribution concerning its tolerance to sea water inundation and a wide range of salinity (2–90‰) (Chapman, 1976; Duke, 1992; Smith, 1992). Previous studies have reported its presence across in landward areas, such as Makoba bay in Zanzibar, Gazi bay in Kenya and Australia (Martínez-Díaz and Reef, 2023; Nitto et al., 2014; Punwong et al., 2013c), This appearance, coupled with the dominance of *A. marina* cover at the SML coring site (Fig. 3), which is connected to an area predominantly covered by grassland, suggests that the presence of *A. marina* in this location may indicate a sea-level fall. This evidence is further substantiated by the consistent decrease in Ca content. In contrast, there is an observed upward trend in Ti levels, which potentially suggests the presence of terrigenous sediments (Bahr et al., 2005; Nace et al., 2014). The low representation of organic content at the base of the SML-1 zone further supports evidence of sea-level fall during this time. This can be attributed to the initial stages of mangrove establishment, which facilitates the transition of the environment from marine to mangrove. Therefore, there is limited mangrove vegetation cover in the early stages of the mangrove ecosystem in the area, leading to low accumulation of organic matter (Gonneea et al., 2004). The decrease in sea level in this area is linked to the reconstructed declining and/or stable relative sea level observed from 2450 BCE, as documented in Zanzibar, Tanzania (Woodroffe et al., 2015), along with a phase of sea-level fall after the mid-Holocene to 400 – 500 CE, as recorded in Makoba Bay, Zanzibar, Tanzania (Punwong et al., 2013c). Furthermore, there is evidence of a relatively rapid sea-level fall after 2050 BCE recorded along the southern African coastline (Ramsay, 1996a,b).

Moreover, total charcoal content reaches its peak across all size classes during this time. The notable abundance of high charcoal levels suggests a combined influence of regional and local fires, with local fires indicated by the appearance of charcoal fragments larger than 100 µm (Punwong et al., 2018b; Whitlock and Larsen, 2001). This indicates a greater prevalence of fire events in this area (Fig. 10), corresponding to a concurrent arid event across East Africa from 2550 to 1550 BCE (Marchant et al., 2018; Marchant and Hooghiemstra, 2004). These conditions may have been influenced by a combination of hydrological patterns, such as the weakening of the summer monsoon and negative Indian Ocean Dipole events (Marchant and Hooghiemstra, 2004; Schreck and Semazzi, 2004), likely associated with the decline in sea level. However, similar to this study, long-term reconstruction faces challenges in clarifying the complex factors in specific areas through sediment cores. This period also marks the gradual transition from a wet to arid climate during the mid to late Holocene in East Africa, spanning 3050–1550 BCE (Liu et al., 2017), which aligns with regional drought phases that emerged across tropical Africa, initiating around 2550–2150 BCE (Hassan, 1997; Kiage and Liu, 2006; Rijsdijk et al., 2011; Stager et al., 2003; Thompson et al., 2002). The weakening of summer monsoon events during the early to mid-Holocene may have been a significant factor causing these drought events across East Africa (An et al., 1993; Gasse and Van Campo, 1994; Kiage and Liu, 2006; Overpeck et al., 1996). A decline in the strength of the summer monsoon could be associated with a reduction in the North Atlantic Sea surface temperatures (SST) (Gasse and Van Campo, 1994), which, in turn, would lead to decreased moisture levels in the African monsoonal airflow responsible for transporting water vapour from the southern subtropical Atlantic anticyclone (Marchant and Hooghiemstra, 2004).

4.1.2. *Period from ~90 BCE – 1700 CE (2040–250 cal yr BP)*

After approximately 90 BCE, *S. alba* exhibited its highest abundance near the top of the SML-1 zone, until approximately 320 CE. Increasing concentrations of silt and reduced sand particles were contemporaneous with these vegetation shifts. This occurrence possibly indicates a brief

period of sea-level rise between 90 BCE and 320 CE (Fig. 10). Moreover, the increasing Fe/S ratio indicates sediment domination by marine influences, further supporting evidence of sea-level rise during this period. This record relates to the deceleration rate of sea-level rise observed in Makoba Bay, Zanzibar, from the mid-Holocene period until 500 CE (Punwong et al., 2013c), as well as a significant sea-level transgression event documented in Unguja Ukuu, Zanzibar, spanning 1800–600 CE (Englong et al., 2023). Following this period, between 320 and 1400 CE in the SML-2 zone, mangrove taxa continued to dominate. However, there was a marked decline in the presence of *S. alba*, while the prevalence of the landward mangrove species *Bruguiera/Ceriops* steadily increased toward the uppermost part of the SML-2 zone. These trends are indicative of a lower sea level (Figs. 9 and 10), corresponding to a period of sea-level regression occurring around 550–750 CE in Tanzania (Punwong et al., 2018a) and in northeastern South Africa after 550 CE (Ramsay and Cooper, 2002). Additionally, a late Holocene sea-level decline after 400 CE in Makoba Bay, Zanzibar, Tanzania (Punwong et al., 2013c) and a potentially low sea level recorded between 1050 and 1150 CE in East Africa (Morner, 2000) further support this evidence. In continuation, *Bruguiera/Ceriops* displayed a continuous increase that extended almost to the middle of the SML-3 zone. In contrast, *R. mucronata* showed a marked decline, and *S. alba* was absent, during this period. Concurrently, non-mangrove arboreal and terrestrial herbaceous taxa, notably Poaceae and Cyperaceae, also exhibited an increase, possibly due to the lower influence of inundation frequency. This suggests a lower sea level compared with the previous period after approximately 1400 CE (Fig. 9). This further deduction is substantiated by the concurrent decrease in clay particles coupled with a concomitant increase in sand particles as well as the ascending trend exhibited by the Ti/Zr ratio. The temporal sequence of rising and falling sea levels during this period indicates significant sea-level fluctuations, predominantly marked by a notable decline from approximately 320 to 1400 CE and a lower sea-level fall extending to 1570 CE in this area (Fig. 10). This is supported by evidence of sea-level fluctuations and lower-than-present MSL, recorded from approximately 850 to 1650 CE in the Kariega estuary along the southern African coast (Strachan et al., 2014), a regression of sea level on the Kenyan coast after 1450 CE (Åse, 1981), and documented instances of reduced sea levels in Zanzibar, Tanzania, from 1300 to 1700 CE (Englong et al., 2023).

Considering a lower sea level after 1400 CE, this drove the reduction of tidal influence, leading the mangrove ecosystem to migrate towards the shore. This episode of decreased sea level resulted in the displacement of the core SML away from the shoreline towards an inland mangrove area (Fig. 9). This transition led to the displacement of seaward mangrove species by landward mangrove species, *Bruguiera/Ceriops*, and Poaceae, demonstrating the capacity to thrive within the newly established landward conditions. The combined factors, including the lower elevation of the SML position compared to the surrounding area (Fig. 2), the prevalence of *A. marina* and *Bruguiera/Ceriops*, and the presence of brownish-yellow sediment colour, potentially indicate that this site evolved into supporting basin mangroves with reduced water flow caused by infrequent sea-level inundation starting from around 1550 CE and continuing onwards. Basin mangroves are typically found in areas situated behind fringing or riverine mangroves, and experience less frequent inundation (Ewel et al., 1998), which corresponds to the SML location (Figs. 2 and 9). The sedimentation rate in the core SML increases notably from the SML-3 to SML-5 zones (0.77–0.88 mm year^{-1}), surpassing that in the lower section (0.15–0.16 mm year^{-1}), may be attributed to local processes associated with the transition into a basin area, facilitating the deposition of both allochthonous and autochthonous sediments due to the low-lying topography. This period of sea-level fall at core SML is a cross-core similarity with the core SMR dated at around 1430 CE. At the bottom of core SMR, the appearance of coral rags and the highest Ca and carbonate contents suggest that the site may have been submerged in seawater and was not vegetated prior to 1430 CE.

In the core SMR, mangrove taxa, particularly *R. mucronata*, followed by *S. alba* and *Bruguiera/Ceriops*, were dominant, whereas Poaceae also appeared and exhibited fluctuations throughout SMR-1 zone, indicating a decrease in sea level, which may have enabled the establishment of mangroves later in the SMR from approximately 1430 CE (Fig. 9). Mangroves at the SMR site occur close to the shoreline, where they are subjected to greater tidal influence. This is associated with the dominance of *R. mucronata* throughout the core, as this species typically thrives in tidal zones and is submerged in all tides (Macnae and Kalk, 1962). Furthermore, an evidence of sea-level fall was supported by a small ruin (Figs. 2 and 9) in the mangrove area adjacent to the core SMR location. As documented by Horton et al. (2017), this ruin was identified as the Mnara mosque, which was constructed in the 15th century CE on a small island located approximately 30 m from the shoreline. The mosque was accessed during low tide by crossing muddy flats; however, it was surrounded by water during the high tide. From the archaeological data of the Mnara mosque, it can be inferred that the sea level in this area was falling during the time of its construction and flourishing around the 15th century CE, which may coincide with the period of human occupation (Fleisher, 2014; Fleisher and Sulas, 2015; Wynne-Jones, 2013) and establishment of mangroves in this area. From 1570 to 1700 CE, *R. mucronata* and *S. alba* increased, while *A. marina* and *Bruguiera/Ceriops* decreased in the core SML. Moreover, Cyperaceae pollen also disappeared during this period. Clay and silt particles increased, while sand particles reduced in cores SML and SMR. These changes align with lower Ti/Zr and higher Fe/S ratios, suggesting a brief episode of sea-level rise (Fig. 10). This specific sea-level rise is a constituent of a broader upward trend noted from 1250 CE to the present day, as evidenced in the salt marsh of southern Langebaan Lagoon, South Africa (Compton, 2001). However, this rise contrasts with reduced sea levels along the Tanzania coast from 1300 to 1850 CE (Englong et al., 2023; Punwong et al., 2018a), and findings from terraces along the Kenyan coast showed relative sea-level decline over the last 500 years (Åse, 1981).

In addition, Cyperaceae pollen is less common in the basal part of the SML-3 zone. Charcoal content slightly increased at the basal part of the SML-3 zone and had a high representation in the middle of the SMR-1 zone, spanning from approximately 1500 to 1610 CE. Coupled with a peak of Poaceae pollen at depths ranging from 58 to 54 cm in the core SMR and the presence of a brownish-yellow colour throughout the core SML from 70 cm onwards, this indicates that the area experienced less frequent and prolonged flooding, both from tidal and freshwater sources, due to drier conditions during the period between 1500 and 1610 CE (Fig. 10). This dry period may have coincided with a minor drought period that occurred between 1560 and 1625 CE in the generally wet climate of the Little Ice Age (~1270 – 1850 CE) (Verschuren et al., 2000), and with drought conditions reconstructed at Lake Edward, central Africa between 1050 and 1650 CE (Russell and Johnson, 2005). It should be noted that during this period of 1300 – 1570 CE, the charcoal content in the core SML was lower than that in both the previous period and the core SMR. This decrease is possibly attributable to the reduced mangrove woods but increased Poaceae in the core SML during this period, which resulted in reduced fuel availability for fires and, subsequently, less fires (Nguyen et al., 2023; Umbanhowar et al., 2009).

4.1.3. Period from ~1700 CE – to the present day (250 cal yr BP – to the present day)

After 1700 CE, mangrove taxa notably decreased, whereas terrestrial herbaceous species, including Cyperaceae and Poaceae pollen, sharply increased in zones SML-4 and SMR-2. This vegetation shift is associated with a consistent decline in silt and increase in sand particles in the lower SML-4 and throughout the SMR-2 zone. Furthermore, an ascending trend in the Ti/Zr ratio in both cores provides further relation with the observed vegetation shift and particle dynamics during this period. These interrelated variables potentially suggest a subsequent sea-level fall around 1700 CE (Figs. 9 and 10). This reinforcing evidence

gains additional support from the decline in sea levels in Zanzibar, Tanzania, covering the period from 1700 to 1900 CE (Englong et al., 2023). It is also a constituent of the extensively documented sea level retreat along the Tanzanian coastline between 1450 and 1850 CE (Punwong et al., 2018a).

From 1870 CE onwards, at the base of zones SML-5 and SMR-3, there was a notable increase in mangrove taxa and a decrease in non-mangrove arboreal and terrestrial herbaceous plants compared to the previous zone. These shifts in pollen composition, coupled with a sudden reduction in sand and an increase in silt particles, may indicate a rise in sea level (Figs. 9 and 10). Subsequently, *R. mucronata* significantly decreased before increasing in the uppermost part of the SMR-3 zone, contrasting with the pattern observed for *Bruguiera/Ceriops*. *S. alba* was present in the uppermost parts of both cores. However, *A. marina* is sharply increased only at the topmost part of the core SML, which contributes to a higher density of pneumatophores, and may also be related to an enhanced sedimentation rate in the uppermost part of core SML (0.88 mm year^{-1}), which is higher than that in previous section (Blasco et al., 1996). These pollen records may suggest a fluctuation in sea level over the past two centuries and a recent rise in sea level at present day (Figs. 9 and 10). The fluctuations in sea level in this area since 1870 CE were concurrent with Holocene sea-level variations observed along the Tanzanian coast in recent centuries (Punwong et al., 2018a). Additionally, a similar trend has been revealed in sea-level changes recorded in Zanzibar, Tanzania, dating from 1700 CE to the present (Englong et al., 2023). The signal of a recent sea level record in this study is closely associated with a global mean sea level rise of 0.20 m during the period from 1901 to 2018 CE (Delmotte et al., 2022).

In addition to the sea-level evidence, the total charcoal content gradually declined and only peaked once more in the upper part of the SMR-2 zone between approximately 1800 and 1850 CE. This peak is linked to a decrease in Cyperaceae pollen in the topmost SML-4 zone and a high representation of Poaceae pollen observed in both SML-4 and SMR-2 zones during the same period. This finding suggests that the area experienced dry conditions, possibly attributed to the broader, drier climate prevalent across East Africa between 1800 and 1850 CE (Fig. 10). This climate pattern may be driven by atmospheric mechanisms closely connected to deviations in Indian Ocean sea-surface temperatures (Bessems et al., 2008; Marchant et al., 2018; Nicholson, 2000; Ryner et al., 2008; Tierney et al., 2013).

A low representation of total charcoal content and Poaceae pollen was observed at the bottom of the SML-5 and SMR-3 zones, along with a high presence of Cyperaceae in the SML-5 zone, which occurred after approximately 1870 CE, possibly suggesting fewer fires due to wetter conditions during this period. This finding corresponds to a wetter phase and a short period of increased rainfall that occurred in East Africa during the late eighteenth century (1860 – 1880 CE) (Marchant et al., 2018; Nicholson, 1996). The total charcoal content showed an increasing trend at the topmost of both SML-5 and SMR-3 zones, coinciding with a slight reduction in Cyperaceae in the uppermost part of the SML-5 zone. This suggests that more fires could relate to the climate in the area becoming dry again from the early nineteenth century to the present (Fig. 10). This finding is consistent with the arid climatic conditions observed in other coastal areas of Tanzania such as Unguja Ukuu, Zanzibar (Englong et al., 2023). This evidence is also in line with the contemporary phase of human-induced climate change, known as the Current Warm Period (CWP), spanning from 1900 CE to the present (Mann et al., 2009; PAGES 2k Consortium, 2019).

4.2. Human interactions with environmental changes in Songo Mnara

Apart from palaeoenvironmental interpretation, sediment records obtained from mangrove cores, along with soil samples, appeared to be indicative of human activity in the area, consistent with the earliest human occupation of Songo Mnara dated from the late 14th to early 16th centuries (Fleisher, 2014; Fleisher and Sulas, 2015). The presence of charcoal fragments greater than 100 μm in the SMR-1 zone after 1580 CE indicates nearby fires (Tinner and Hu, 2003), as observed in this study near a mangrove area. The occurrence of the largest charcoal fragments (>150 μm) during the same period supports an increase in local fires (Carcaillet et al., 2001; Rucina et al., 2009) within mangroves. This finding is consistent with the massive occurrence of charcoal fragments larger than 100 μm found in soil samples collected from cultural layers during the 14th and 16th centuries CE in an open area close to the core SMR. The positive association between increased charcoal and the presence of C3-Pooideae and C-4 Panicoideae phytoliths in both sediment cores and soil samples suggests that Songo Mnara was significantly affected by anthropogenic activities during this time (Fig. 10). These findings possibly suggest that humans have utilised controlled fires for land clearance to create space for their activities, such as cultivation or the construction of residences (Bowman et al., 2011). This period coincided with period of falling sea levels, beginning around 320–1570 CE and associated with human activity from approximately 1430 CE, may have led to the broad expansion of low coastal landforms. This expansion potentially represents one of the contributing factors that facilitates greater access to marine resources for the local population (Pollard, 2009). The elevated Ca levels detected in all soil samples may be attributed to the occurrence of shell fragments and shell beads (Fleisher and Sulas, 2015). The creation of shell beads involves the grinding of shells (Flexner et al., 2008), resulting in the formation of fine debris rich in calcium. This suggests the exploitation of marine resources for consumption and bead production (Pawlowicz et al., 2023), providing further evidence of human activities.

In addition, the soil samples indicated the presence of bilobate and cross morphotypes recognised as C4-Panicoideae, as well as a trapezoid morphotype recognised as C3-Pooideae (Mustaphi et al., 2021; Neumann et al., 2017). The occurrence of C4-Panicoideae phytoliths is potentially associated with native African cereals, such as domesticated pearl millet, sorghum, and finger millet. These crops have been identified as significant food resources in Songo Mnara, based on the presence of macrobotanical remains (Morales et al., 2022). Certain phytolith morphotypes of the C3-Pooideae may be connected to Asian rice (McParland and Walshaw, 2015), which may have been introduced into East Africa through trade across the Indian Ocean (Boivin et al., 2013). After around 1600 CE, charcoal fragments greater than 150 μm in size disappeared at the core SMR, suggesting a reduction in local fires, possibly caused by human abandonment from the early 16th century (Fig. 10). There is no clear evidence to explain the abandonment of humans in Songo Mnara during this period, although it coincides with the arrival of the Portuguese at Kilwa, their control over the town, and trade passing through it. However, it is possible that a drought regime between 1500 and 1612 CE, followed by a brief period of sea-level rise between 1570 and 1720 CE, as revealed in our records, is related to this abandonment. Archaeological records suggest that the inhabitants of this area rely on natural springs and wells for their daily needs and agricultural activities (Fleisher, 2014; Holliday and Gartner, 2007; Sulas et al., 2017), which in turn are indicative of their food resources. Therefore, if drought conditions occur and cause a shortage of natural freshwater, this could have led to a shortage of food resources. Combined with evidence of sea-level rise, which also influenced the decrease accessibility of marine food resources, this may have resulted in human abandonment in the area.

After 1870 CE, higher charcoal levels may be related to the re-settlement of humans after abandonment in the early 16th century (Fig. 10). Songo Mnara was once again occupied by an agricultural village on the southern part of the island and persisted until the recent day (Wynne-Jones and Fleisher, 2015). This record is related to the appearance of charcoal fragments larger than 150 μm at the top part of the core SMR, which dates to around 1950 CE. The presence of charcoal during this period may be attributed to the extensive utilisation of mangrove wood for the production of charcoal, firewood, fuel, and construction materials by human populations commonly found along

the East African coast (Englong et al., 2023; Ngoile and Shunula, 1992; Semesi, 1998), including Songo Mnara (Pawlowicz et al., 2023). This anthropogenic activity may have contributed to a slight reduction in the abundance of *S. alba* and *R. mucronata* from approximately 100 years ago, despite the majority of sedimentary records, especially pollen records, indicating evidence of recent sea-level rise. Limited evidence of human activity in the Songo Mnara area suggests that any practice is likely to have been local with no evidence of industrial activities.

5. Conclusion

Examining palaeoenvironmental data within the mangroves sedimentary and cultural soil records of Songo Mnara not only indicates past environmental change over the past four millennia but also reveals the interaction between the coastal environment and human populations, especially in response to sea-level and climate changes. The presence of coral rags and the high calcium content in the deepest layers of the sediment cores indicate a lack of vegetation due to high sea levels before 2590 BCE. Subsequent increases of mangrove taxa indicated a sea-level fall facilitating the establishment of mangroves in areas previously influenced by marine tidal waters from 2590 BCE to 90 CE. This aligns with regional sea-level patterns and arid climatic events during the mid to late Holocene. From approximately 90 BCE to 320 CE, the presence of seaward mangrove species suggested a brief sea-level rise phase, followed by a lower sea level indicated by a transition from seward to landward mangrove species until ~1400 CE. After that, the records indicate that sea level was further reduced compared to the previous period. During the period from around 1400 CE, significant human activity in Songo Mnara is evidenced by the presence of charcoal fragments and C3-Pooideae and C-4 Panicoideae phytoliths potentially associated with native African cereals, such as domesticated pearl millet, sorghum, finger millet, and Asian rice. This implies controlled fires potentially linked to agricultural practices and resource utilisation. This also coincides with sea-level fall, which likely enhances the exploitation of marine resources. These findings align with archaeological evidence indicating human settlement on the island from the late 14th century to the early 16th century CE, signifying a period of human-environment interaction on the island. Subsequent sea-level rise and possible drought conditions, which affected the availability of freshwater and marine resources, may have contributed to the abandonment of the island in the early 16th century CE. From 1700 CE, the sedimentary records suggest fluctuations in sea level with evidence of both rise and fall, mirroring documented sea-level changes along the Tanzanian coast and broader climatic trends. The recent sea-level rise, consistent with global trends, is observable in records from approximately 1870 CE to the present day. This period also revealed the reoccupation of the island by human populations, with a particular focus on the utilisation of mangrove resources. However, this activity does not appear to involve large-scale industrial processes and the heavy metal content remains low, indicating effective conservation efforts.

It should be noted that Songo Mnara Island is susceptible to sea-level rise. Projected global sea-level rise, ranging from 3.0 to 13.2 mm year^{-1} by 2100 CE under low to high greenhouse gas emission scenarios (Horton et al., 2020), coupled with lower sedimentation rates of 0.15–1.32 mm year^{-1} within mangrove areas, suggests that the mangroves on Songo Mnara may struggle to keep pace with the current rate of sea-level rise. This vulnerability could have profound implications for the island, particularly for its coastal archaeological sites, which are listed as UNESCO World Heritage Sites. As a result, our records hold significant potential for informing the development of strategies aimed at safeguarding mangrove forests and coastal communities from the impacts of sea-level rise. Additionally, these findings may contribute to ongoing conservation efforts for this World Heritage Site and offer insights applicable to other low-lying islands that face similar challenges.

CRediT authorship contribution statement

Apichaya Englong: Writing – review & editing, Writing – original draft, Visualization, Project administration, Methodology, Investigation, Formal analysis, Data curation, Conceptualization. **Paramita Punwong:** Writing – review & editing, Supervision, Methodology, Investigation, Data curation, Conceptualization. **Tosak Seelanan:** Writing – review & editing, Supervision, Investigation, Funding acquisition, Conceptualization. **Rob Marchant:** Writing – review & editing, Supervision, Investigation, Conceptualization. **Stephanie Wynne-Jones:** Writing – review & editing, Supervision, Data curation. **Akkaneewut Jirapinyakul:** Writing – review & editing, Supervision, Methodology. **Jeffrey Fleisher:** Writing – review & editing, Data curation.

Declaration of competing interest

The authors declare that they have no actual, potential or perceived conflict of interest in relation to influence the work reported in this paper.

Data availability

No data was used for the research described in the article.

Acknowledgements

We would like to express our gratitude to Rebecca Newman and Malekano Malindi for their support and assistance throughout this fieldwork. Appreciation is expressed in the Songo Mnara Urban Landscape Project for providing soil samples. This research was conducted in collaboration with the Antiquities Division, Ministry of Natural Resources and Tourism, Tanzania, which kindly granted permission for sediment collection. Our special thanks go to Dr. Federica Sulas for provided valuable comments and suggestions on this manuscript, Dr. Luke Andrews for laboratory assistance and Kamonpan Anglong for the illustrations. We are grateful to the Department of Geology, Chulalongkorn University for kindly lending a handheld XRF analyser. The authors would like to acknowledge the Synchrotron Light Research Institute (Public Organization), SLRI, for the provision of additional dating. This research was supported by the Science Achievement Scholarship of Thailand (SAST) from the Ministry of Higher Education, Science, Research, and Innovation and by a CU Graduate School Thesis Grant.

Appendix A. Supplementary data

Supplementary data to this article can be found online at https://doi.org/10.1016/j.qsa.2024.100192.

References

Adojoh, O.C., Marret, F., Duller, R., Osterloff, P.L., Oboh-Ikuenobe, F.E., Saylor, B.Z., 2023. Stages of palaeoenvironmental evolution, climate and sea level change of the Niger Delta, east Equatorial Atlantic: novelty from elemental tracers, sedimentary facies and pollen records. Holocene, 09596836231163506.

An, Z., Porter, S.C., Weijian, Z., Yanchou, L., Donahue, D.J., Head, M.J., Xihuo, W., Jianzhang, R., Hongbo, Z., 1993. Episode of strengthened summer monsoon climate of Younger Dryas age on the Loess Plateau of Central China. Quat. Res. 39, 45–54.

Arthurton, R., 2003. The fringing reef coasts of eastern Africa—present processes in their long-term context. West. Indian Ocean J. Mar. Sci. 2 (1), 1–14.

Åse, L.E., 1981. Studies of shores and shore displacement on the southern coast of Kenya—especially in Kilifi District. Geogr. Ann. Phys. Geogr. 63 (3–4), 303–310.

Bahr, A., Lamy, F., Arz, H., Kuhlmann, H., Wefer, G., 2005. Late glacial to Holocene climate and sedimentation history in the NW Black Sea. Mar. Geol. 214 (4), 309–322.

Barboni, D., Bremond, L., 2009. Phytoliths of East African grasses: an assessment of their environmental and taxonomic significance based on floristic data. Rev. Palaeobot. Palynol. 158 (1–2), 29–41.

Behling, H., Cohen, M.C., Lara, R.J., 2001. Studies on Holocene mangrove ecosystem dynamics of the Bragança Peninsula in north-eastern Pará, Brazil. Palaeogeogr. Palaeoclimatol. Palaeoecol. 167 (3–4), 225–242.
Bessems, I., Verschuren, D., Russell, J.M., Hus, J., Mees, F., Cumming, B.F., 2008. Palaeolimnological evidence for widespread late 18th century drought across equatorial East Africa. Palaeogeogr. Palaeoclimatol. Palaeoecol. 259 (2–3), 107–120.
Blaauw, M., Christen, J.A., 2013. Bacon Manual V2. 3.3. Queens University, Belfast.
Blackford, J.J., 2000. Charcoal fragments in surface samples following a fire and the implications for interpretation of subfossil charcoal data. Palaeogeogr. Palaeoclimatol. Palaeoecol. 164, 33–42.
Blasco, F., Saenger, P., Janodet, E., 1996. Mangroves as indicators of coastal change. Catena 27 (3–4), 167–178.
Boivin, N., Crowther, A., Helm, R., Fuller, D.Q., 2013. East Africa and Madagascar in the Indian ocean world. J. World PreHistory 26 (3), 213–281.
Bonny, A.P., 1972. A method for determining absolute pollen frequencies in lake sediments. New Phytol. 71 (2), 393–405.
Bowman, D.M.J.S., Balch, J., Artaxo, P., Bond, W.J., Cochrane, M.A., D'Antonio, C.M., DeFries, R., Johnston, F.H., Keeley, J.E., Krawchuk, M.A., Kull, C.A., Mack, M., Moritz, M.A., Pyne, S., Roos, C.I., Scott, A.C., Sodhi, N.S., Swetnam, T.W., 2011. The human dimension of fire regimes on Earth: the human dimension of fire regimes on Earth. J. Biogeogr. 38 (12), 2223–2236.
Bozi, B.S., Figueiredo, B.L., Rodrigues, E., Cohen, M.C., Pessenda, L.C., Alves, E.E., Culligan, N., 2021. Impacts of sea-level changes on mangroves from southeastern Brazil during the Holocene and Anthropocene using a multi-proxy approach. Geomorphology 390, 107860.
Brock, F., Higham, T., Ditchfield, P., Ramsey, C.B., 2010. Current pretreatment methods for AMS radiocarbon dating at the Oxford radiocarbon accelerator unit (Orau). Radiocarbon 52 (1), 103–112.
Carcaillet, C., Bouvier, M., Fréchette, B., Larouche, A.C., Richard, P.J.H., 2001. Comparison of pollen-slide and sieving methods in lacustrine charcoal analyses for local and regional fire history. Holocene 11 (4), 467–476.
Castañeda-Posadas, C., Correa-Metrio, A., Escobar, J., Moreno, J.E., Curtis, J.H., Blaauw, M., Jaramillo, C., 2022. Mid to late Holocene sea-level rise and precipitation variability recorded in the fringe mangroves of the Caribbean coast of Panama. Palaeogeogr. Palaeoclimatol. Palaeoecol. 592, 110918.
Chapman, V.J., 1976. Mangrove Vegetation. J. Cramer, Vaduz.
Chittick, H.N., 1974. Kilwa: an Islamic Trading City on the East African Coast. British Institute in Eastern Africa, Nairobi and London.
Chumchim, N., 2010. Palynology of Mangrove Flora in Thailand. Chulalongkorn University, Bangkok. Master thesis in Botany, Graduate School.
Clark, R.L., 1982. Point count estimation of charcoal in pollen preparations and thin sections of sediments. Pollen Spores 24, 523–535.
Clark, J.S., 1988a. Particle motion and the theory of stratigraphic charcoal analysis: source area, transport, deposition and sampling. Quat. Res. 30, 67–80.
Clark, J.S., 1988b. Stratigraphic charcoal analysis on petrographic thin sections: application of fire history in Northwestern Minnesota. Quat. Res. 30, 81–91.
Clark, J.S., Merkt, J., Muller, H., 1989. Post-glacial fire, vegetation and human history on the northern Alpine forelands, south-west Germany. J. Ecol. 77, 897–925.
Coe, H.H.G., Souza, R.C.C.L., Duarte, M.R., Ricardo, S.D.F., Machado, D.O.B.F., Macario, K.C.D., Silva, E.P., 2017. Characterisation of phytoliths from the stratigraphic layers of the Sambaqui da Tarioba (Rio das Ostras, RJ, Brazil). Flora 236–237, 1–8.
Cohen, M.C.L., Camargo, P.M.P., Pessenda, L.C.R., Lorente, F.L., De Souza, A.V., Corrêa, J.A.M., Bendassolli, J., Dietz, M., 2021. Effects of the middle Holocene high sea-level stand and climate on Amazonian mangroves. J. Quat. Sci. 36 (6), 1013–1027.
Color, M., 2009. Munsell soil color charts. Munsell Soil Color Charts, pp. 1–23.
Compton, J.S., 2001. Holocene sea-level fluctuations inferred from the evolution of depositional environments of the southern Langebaan Lagoon salt marsh, South Africa. Holocene 11 (4), 395–405.
Delmotte, V., Zhai, P., Pörtner, H.O., Roberts, D., Skea, J., Shukla, P.R., 2022. Global Warming of 1.5 C: IPCC special report on impacts of global warming of 1.5 C above pre-industrial levels in context of strengthening response to climate change. Sustainable Development, and Efforts to Eradicate Poverty. Cambridge University Press, pp. 1–632.
Doktorgrades, E., 2004. Reconstruction of the Sedimentary Environment and Climate Conditions by Multi-Geochemical Investi- Gations of Late Palaeozoic Glacial to Postglacial Sedimentary Sequences from SW-Gondwana, pp. 96–117. Dissertation submitted to Universitat Bonn, Germany.
Duke, N.C., 1992. Mangrove floristics and biogeography. In: Robertson, A.I., Alongi, D. M. (Eds.), Tropical Mangrove Ecosystems, American Geophysical Union, pp. 63–100. Washington DC.
Ellison, J.C., 2015. Vulnerability assessment of mangroves to climate change and sea-level rise impacts. Wetl. Ecol. Manag. 23 (2), 115–137.
Ellison, J., Strickland, P., 2015. Establishing relative sea level trends where a coast lacks a long-term tide gauge. Mitig. Adapt. Strategies Glob. Change 20 (7), 1211–1227.
Englong, A., Punwong, P., Marchant, R., Seelanan, T., Wynne-Jones, S., Chirawatkul, P., 2023. High-resolution multiproxy record of environmental changes and anthropogenic activities at Unguja Ukuu, Zanzibar, Tanzania during the last 5000 years. Quaternary 6 (1), 21.
Erdtman, G., 1969. Handbook of palynology: morphology, TaxonomyEcology. Preis, Copenhagen, p. 486.
Ewel, K.C., Twilley, R.R., Ong, J.E., 1998. Different kinds of mangrove forests provide different goods and services. Global Ecol. Biogeogr. Lett. 7 (1), 83.
Faegri, K., Iversen, J., 1989. Textbook of Pollen Analysis. Wiley and Sons, Chichester.
Fleisher, J., 2014. The complexity of public space at the Swahili town of Songo Mnara, Tanzania. J. Anthropol. Archaeol. 35, 1–22.
Fleisher, J., Sulas, F., 2015. Deciphering public spaces in urban contexts: geophysical survey, multi-element soil analysis, and artifact distributions at the 15th–16th-century AD Swahili settlement of Songo Mnara, Tanzania. J. Archaeol. Sci. 55, 55–70.
Fleisher, J., Wynne-Jones, S., 2012. Finding meaning in ancient Swahili spatial practices. Afr. Archaeol. Rev. 29 (2–3), 171–207.
Flexner, J.L., Fleisher, J.B., LaViolette, A., 2008. Bead grinders and Early Swahili household economy: analysis of an assemblage from Tumbe, Pemba Island, Tanzania, 7th-10th centuries AD. J. Afr. Archaeol. 6, 161–181.
Fontes, N.A., Moraes, C.A., Cohen, M.C.L., Alves, I.C.C., França, M.C., Pessenda, L.C.R., Francisquini, M.I., Bendassolli, J.A., Macario, K., Mayle, F., 2017. The impacts of the middle Holocene high Sea-Level stand and climatic changes on mangroves of the Jucuruçu river, southern Bahia – northeastern Brazil. Radiocarbon 59 (1), 215–230.
Gao, G., Wang, M., Li, D., Li, N., Wang, J., Niu, H., Meng, M., Liu, Y., Zhang, G., Jie, D., 2023. Phytolith evidence for changes in the vegetation diversity and cover of a grassland ecosystem in Northeast China since the mid-Holocene. Catena 226, 107061.
Gasse, F., van Campo, E., 1994. Abrupt post-glacial climatic events in West Asian and North African monsoon domains. Earth Planet Sci. Lett. 26, 435–456.
Gilman, E.L., Ellison, J., Duke, N.C., Field, C., 2008. Threats to mangroves from climate change and adaptation options: a review. Aquat. Bot. 89 (2), 237–250.
GISGeography, 2023. https://gisgeography.com/tanzania-map/. (Accessed 5 August 2023).
Gonneea, M.E., Paytan, A., Herrera-Silveira, J.A., 2004. Tracing organic matter sources and carbon burial in mangrove sediments over the past 160 years. Estuar. Coast Shelf Sci. 61 (2), 211–227.
Google, 2022. Map of Songo Mnara). Retrieved January 19, 2022, from. https://earth.google.com/web/@9.07236762,39.58822901,11.54785909a,18364.94918656d,34.99260148y,0h,0t,0r.
Grimm, E.C., 1991. Tilia and Tiliagraph. Illinois State Museum, Springfield.
Hapsari, K.A., Ballauff, J., 2022. Distinguishing pollen grains of cereal from wild grasses in the Sundaland region using size separation. Rev. Palaeobot. Palynol. 301, 104648.
Harvey, E.L., Fuller, D.Q., 2005. Investigating crop processing using phytolith analysis: the example of rice and millets. J. Archaeol. Sci. 32 (5), 739–752.
Hassan, F.A., 1997. Holocene palaeoclimates of Africa. Afr. Archaeol. Rev. 14 (4), 213–230.
Havinga, A.J., 1967. Palynology and pollen preservation. Rev. Palaeobot. Palynol. 2 (1–4), 81–98.
Heiri, O., Lotter, A.F., Lemcke, G., 2001. Loss on ignition as a method for estimating organic and carbonate content in sediments: reproducibility and comparability of results. J. Paleolimnol. 25, 101–110.
Hogg, A.G., Heaton, T.J., Hua, Q., Palmer, J.G., Turney, C.S., Southon, J., Bayliss, A., Blackwell, P.G., Boswijk, G., Bronk Ramsey, C., Pearson, C., Petchey, F., Reimer, P., Reimer, R., Wacker, L., 2020. SHCal20 southern Hemisphere calibration, 0–55,000 Years cal BP. Radiocarbon 62 (4), 759–778.
Holliday, V.T., Gartner, W.G., 2007. Methods of soil P analysis in archaeology. J. Archaeol. Sci. 34 (2), 301–333.
Horton, M., Fleisher, J., Wynne-Jones, S., 2017. The mosques of Songo Mnara in their urban landscape. J. Islamic Archaeol. 4 (2), 163–188.
Horton, B., Khan, N., Cahill, N., Lee, J., Shaw, T., Garner, A., Rahmstorf, S., 2020. Estimating global mean sea-level rise and its uncertainties by 2100 and 2300 from expert assessment. In: EGU General Assembly Conference Abstracts, p. 7302.
Hunt, C.O., Fieller, N.R.J., Gilbertson, D.D., Ralph, N.G.A., 1985. Recent advances in pollen extraction techniques: a brief review. Palaeobiol. Investig. 266, 181–187.
Indeje, M., Semazzi, F.H.M., Ogallo, L.J., 2000. ENSO signals in East African rainfall seasons. Int. J. Climatol. 20 (1), 19–46.
Joly, C., Barillé, L., Barreau, M., Mancheron, A., Visset, L., 2007. Grain and annulus diameter as criteria for distinguishing pollen grains of cereals from wild grasses. Rev. Palaeobot. Palynol. 146 (1–4), 221–233.
Kakroodi, A.A., Leroy, S.A.G., Kroonenberg, S.B., Lahijani, H.A.K., Alimohammdian, H., Yamani, M., Nohegar, A., 2012. Late Pleistocene and Holocene sea level-change and coastal palaeoenvironment along the Iranian Caspian shore. Earth Planet Sci. Lett. *submitted for publication*.
Kershaw, A.P., 1997. A modification of the Troels–Smith system of sediment description and portrayal. Quat. Australasia 15 (2), 63–68.
Kiage, L.M., Liu, K., 2006. Late Quaternary paleoenvironmental changes in East Africa: a review of multiproxy evidence from palynology, lake sediments, and associated records. Prog. Phys. Geogr. Earth Environ. 30 (5), 633–658.
Limaye, R.B., Kumaran, K.P.N., 2012. Mangrove vegetation responses to Holocene climate change along Konkan coast of south-western India. Quat. Int. 263, 114–128.
Liu, X., Rendle-Bühring, R., Henrich, R., 2017. Geochemical composition of Tanzanian shelf sediments indicates Holocene climatic and sea-level changes. Quat. Res. 87 (3), 442–454.
Ma, Q., Zhu, L., Wang, J., Ju, J., Wang, Y., Lü, X., Kasper, T., Haberzettl, T., 2020. Late Holocene vegetation responses to climate change and human impact on the central Tibetan Plateau. Sci. Total Environ. 708, 135370.
Macnae, W., Kalk, M., 1962. The ecology of the mangrove swamps at Inhaca island, Mozambique. J. Ecol. 50 (1), 19–34.
Madella, M., Powers-Jones, A.H., Jones, M.K., 1998. A simple method of extraction of opal phytoliths from sediments using a non-toxic heavy liquid. J. Archaeol. Sci. 25 (8), 801–803.
Mann, M.E., Zhang, Z., Rutherford, S., Bradley, R.S., Hughes, M.K., Shindell, D., Ammann, C., Faluvegi, G., Ni, F., 2009. Global signatures and dynamical origins of the little Ice age and medieval climate anomaly. Science 326 (5957), 1256–1260.

Marchant, R., Hooghiemstra, H., 2004. Rapid environmental change in African and South American tropics around 4000 years before present: a review. Earth Sci. Rev. 66 (3–4), 217–260.
Marchant, R., Richer, S., Boles, O., Capitani, C., Courtney-Mustaphi, C.J., Lane, P., Prendergast, M.E., Stump, D., De Cort, G., Kaplan, J.O., Phelps, L., Kay, A., Olago, D., Petek, N., Platts, P.J., Punwong, P., Widgren, M., Wynne-Jones, S., Ferro-Vázquez, C., Wright, D., 2018. Drivers and trajectories of land cover change in East Africa: human and environmental interactions from 6000 years ago to present. Earth Sci. Rev. 178, 322–378.
Martínez-Díaz, M.G., Reef, R., 2023. A biogeographical approach to characterizing the climatic, physical and geomorphic niche of the most widely distributed mangrove species, *Avicennia marina*. Divers. Distrib. 29 (1), 89–108.
McClanahan, T., 1988. Seasonality in East Africa's coastal waters. Mar. Ecol. Prog. Ser. 44, 191–199.
McParland, H.J., 2017. A spatial approach to Phytolith analysis for the detection of interior and exterior spaces at Songo Mnara. *Tanzania* (Doctoral Dissertation. University of York.
McParland, H., Walshaw, S., 2015. Swahili plant use and activity areas at Songo Mnara, Tanzania: a case study at macro and micro scales. Societa dei Nat-uralisti e Matematici di Modena, Suppl 146, 193–195.
Mendoza, U.M., 2007. *Dynamics of Phosphorus and Sulphur in a Mangrove Forest in Bragança, North Brazil* (Doctoral Dissertation. Universität Bremen).
Mercader, J., Bennett, T., Esselmont, C., Simpson, S., Walde, D., 2009. Phytoliths in woody plants from the Miombo woodlands of Mozambique. Ann. Bot. 104 (1), 91–113.
Moraes, C.A., da Costa, M.L., Navarro, A.G., da Silva Meneses, M.E.N., Negrão, L.B.A., Pöllmann, H., Behling, H., 2021. Holocene coastal environmental changes inferred by multi-proxy analysis from Lago Formoso sediments in Maranhão State, northeastern Brazil. Quat. Sci. Rev. 273, 107234.
Morales, E.M.Q., Craig, O.E., Prendergast, M.E., Walshaw, S., Cartaciano, C., Mwebi, O., Wynne-Jones, S., 2022. Diet, economy, and culinary practices at the height of precolonial Swahili urbanism. J. Anthropol. Archaeol. 66, 101406.
Morner, N.A., 2000. Sea level changes and coastal dynamics in the Indian Ocean. Integrated Coastal Zone Management 17–21. Launch Edition.
Mustaphi, C.J.C., Rucina, S.M., King, L., Selby, K., Marchant, R., 2021. A palaeovegetation and diatom record of tropical montane forest fire, vegetation and hydroseral changes on Mount Kenya from 27,000–16,500 cal yr BP. Palaeogeogr. Palaeoclimatol. Palaeoecol. 581, 110625.
Nace, T.E., Baker, P.A., Dwyer, G.S., Silva, C.G., Rigsby, C.A., Burns, S.J., Giosan, L., Otto-Bliesner, B., Liu, Z., Zhu, J., 2014. The role of North Brazil Current transport in the paleoclimate of the Brazilian Nordeste margin and paleoceanography of the western tropical Atlantic during the late Quaternary. Palaeogeogr. Palaeoclimatol. Palaeoecol. 415, 3–13.
Nakamura, R., 2012. Maritime environments of Swahili civilizations: the mangrove inland sea of Kilwa island, Tanzania. Afro-Eurasian Inner Dry Land Civilizations 1, 81–89.
NASA JPL, 2013. NASA shuttle radar topography mission global 1 arc second. NASA EOSDIS Land Processes DAAC. https://doi.org/10.5067/MEaSUREs/SRTM/SRTMGL1.003. Retrieved July 4, 2023, from.
Neumann, K., Fahmy, A.G., Müller-Scheeßel, N., Schmidt, M., 2017. Taxonomic, ecological and palaeoecological significance of leaf phytoliths in West African grasses. Quat. Int. 434, 15–32.
International Committee for Phytolith Taxonomy (ICPT), Neumann, K., Strömberg, C.A. E., Ball, T., Albert, R.M., Vrydaghs, L., Cummings, L.S., 2019. International Code for Phytolith nomenclature (ICPN) 2.0. Ann. Bot. 124 (2), 189–199.
Ngoile, M.A.K., Shunula, J.P., 1992. Status and exploitation of the mangrove and associated fishery resources in Zanzibar. Hydrobiologia 247, 229–234.
Nguyen, C.H., Hapsari, K.A., Saad, A., Sabiham, S., Behling, H., 2023. Late Holocene riparian vegetation dynamics, environmental changes, and human impact in the Harapan forest of Sumatra, Indonesia. Frontiers in Ecology and Evolution 11, 1224160.
Nicholas, C.J., Pearson, P.N., McMillan, I.K., Ditchfield, P.W., Singano, J.M., 2007. Structural evolution of southern coastal Tanzania since the Jurassic. J. Afr. Earth Sci. 48 (4), 273–297.
Nichols, G.J., 2009. Sedimentology and Stratigraphy. John Wile & Sons, New York.
Nicholson, S.E., 1996. A review of climate dynamics and climate variability in Eastern Africa. In: Johnson, T.C., Odada, E. (Eds.), Limnology, Climatology and Paleoclimatology of the East African Lakes. Gordon & Breach, Amsterdam, pp. 25–56.
Nicholson, S., 2000. The nature of rainfall variability over Africa on time scales of decades to millenia. Global Planet. Change 26 (1–3), 137–158.
Nitto, D., Neukermans, G., Koedam, N., Defever, H., Pattyn, F., Kairo, J.G., Dahdouh-Guebas, F., 2014. Mangroves facing climate change: landward migration potential in response to projected scenarios of sea level rise. Biogeosciences 11 (3), 857–871.
Novello, A., Barboni, D., 2015. Grass inflorescence phytoliths of useful species and wild cereals from sub-Saharan Africa. J. Archaeol. Sci. 59, 10–22.
Overpeck, J., Anderson, D., Trumbore, S., Prell, W., 1996. The southwest Indian monsoon over the last 18000 years. Clim. Dynam. 12, 213–225.
PAGES 2k Consortium, 2019. Consistent multidecadal variability in global temperature reconstructions and simulations over the Common Era. Nat. Geosci. 12 (8), 643–649.
Patterson III, W.A., Edwards, K.J., MacGuire, D.J., 1987. Microscopic charcoal as a fossil indicator of fire. Quat. Sci. Rev. 6, 3–23.
Pawlowicz, M., Fleisher, J., Wynne-Jones, S., 2023. Exploring Swahili urbanism through survey of Songo Mnara island, Tanzania. J. I. Coast Archaeol. 18 (3), 426–450.
Pearsall, D.M., Duncan, N.A., Jones, J.G., Friedel, D.E., Veintimilla, C.I., Neff, H., 2016. Human–environment interactions during the early mid-Holocene in coastal Ecuador as revealed by mangrove coring in Santa Elena Province. Holocene 26 (8), 1262–1289.
Piperno, D.R., Ranere, A.J., Holst, I., Iriarte, J., Dickau, R., 2009. Starch grain and phytolith evidence for early ninth millennium B.P. maize from the Central Balsas River Valley, Mexico. Proc. Natl. Acad. Sci. USA 106 (13), 5019–5024.
Pitkanen, A., Huttunen, P., 1999. A 1300 year forest-fire history at a site in eastern Finland based on charcoal and pollen records in laminated lake sediment. Holocene 9, 311–320.
Pollard, E., 2009. Settlement adaptation to a changing coastline: archaeological evidence from Tanzania, during the first and second millennia AD. J. I. Coast Archaeol. 4 (1), 82–107.
Pollard, E., Fleisher, J., Wynne-Jones, S., 2012. Beyond the stone town: maritime architecture at fourteenth–fifteenth century Songo Mnara, Tanzania. J. Marit. Archaeol. 7 (1), 43–62.
Pouwels, R.L., 2002. Eastern Africa and the Indian ocean to 1800. Reviewing relations in historical perspective. Int. J. Afr. Hist. Stud. 35 (2/3), 385.
Prentice, A.J., Webb, E.A., 2016. The effect of progressive dissolution on the oxygen and silicon isotope composition of opal-A phytoliths: implications for palaeoenvironmental reconstruction. Palaeogeogr. Palaeoclimatol. Palaeoecol. 453, 42–51.
Punwong, P., 2008. Pollen Deposit in Bangkok Clay from Ong Kharak District Nakhon Nayok Province, and Their Implication on Paleo- Phytogeography. Chulalongkorn University, Bangkok. Master thesis in Botany, Graduate School.
Punwong, P., Marchant, R., Selby, K., 2013a. Holocene mangrove dynamics and environmental change in the Rufiji Delta, Tanzania. Veg. Hist. Archaeobotany 22 (5), 381–396.
Punwong, P., Marchant, R., Selby, K., 2013b. Holocene mangrove dynamics from Unguja Ukuu, Zanzibar. Quat. Int. 298, 4–19.
Punwong, P., Marchant, R., Selby, K., 2013c. Holocene mangrove dynamics in Makoba Bay, Zanzibar. Palaeogeogr. Palaeoclimatol. Palaeoecol. 379–380, 54–67.
Punwong, P., Selby, K., Marchant, R., 2018a. Holocene mangrove dynamics and relative sea-level changes along the Tanzanian coast, East Africa. Estuar. Coast Shelf Sci. 212, 105–117.
Punwong, P., Sritrairat, S., Selby, K., Marchant, R., Pumijumnong, N., Traiperm, P., 2018b. An 800 year record of mangrove dynamics and human activities in the upper Gulf of Thailand. Veg. Hist. Archaeobotany 27, 535–549.
Punwong, P., Englong, A., Marchant, R., Jirapinyakul, A., Suttiwong, A., Chirawatkul, P., Promchoo, W., 2024. A multi-proxy reconstruction of the late Holocene vegetation dynamics in Krabi mangroves, Thailand Andaman Sea. Quaternary Science Advances 13, 100133.
Quamar, M.F., Kar, R., 2022. Agricultural practices in India during the Holocene: a pollen view point and a critical appraisal. Holocene 32 (11), 1340–1357.
R Development Core Team, 2015. R: A Language and Environment for Statistical Computing. R version 3.2.0 (accessed April 2023). http://www.r-project.org.
Ramsay, P.J., 1996a. 9000 years of sea-level change along the southern African coastline. Quat. Int. 31, 71–75.
Ramsay, P.J., 1996b. 9000 Years of sea-level change along the southern African coastline. Quat. Int. 31, 71–75.
Ramsay, P.J., Cooper, J.A.G., 2002. Late Quaternary sea-level change in South Africa. Quat. Res. 57 (1), 82–90.
Rhodes, A.N., 1998. A method for the preparation and quantification of microscopic charcoal from terrestrial and lacustrine sediment cores. Holocene 8, 113–117.
Rijsdijk, K.F., Zinke, J., De Louw, P.G.B., Hume, J.P., Van Der Plicht, H.J., Hooghiemstra, H., Meijer, H.J.M., Vonhof, H.B., Porch, N., Florens, F.B.V., Baider, C., Van Geel, B., Brinkkemper, J., Vernimmen, T., Janoo, A., 2011. Mid-Holocene (4200 kyr BP) mass mortalities in Mauritius (Mascarenes): insular vertebrates resilient to climatic extremes but vulnerable to human impact. Holocene 21 (8), 1179–1194.
Rodriguez, E., Morris, C.S., Belz, J.E., 2006. A global assessment of the SRTM performance. Photogramm. Eng. Rem. Sens. 72 (3), 249–260.
Rozan, T.F., Taillefert, M., Trouwborst, R.E., Glazer, B.T., Ma, S., Herszage, J., Valdes, L. M., Price, K.S., Luther Iii, G.W., 2002. Iron-sulfur-phosphorus cycling in the sediments of a shallow coastal bay: implications for sediment nutrient release and benthic macroalgal blooms. Limnol. Oceanogr. 47 (5), 1346–1354.
Rucina, S.M., Muiruri, V.M., Kinyanjui, R.N., McGuiness, K., Marchant, R., 2009. Late Quaternary vegetation and fire dynamics on Mount Kenya. Palaeogeogr. Palaeoclimatol. Palaeoecol. 283 (1–2), 1–14.
Ruiz-Fernández, A.C., Agraz-Hernández, C.M., Sanchez-Cabeza, J.A., Díaz-Asencio, M., Pérez-Bernal, L.H., Chan Keb, C.A., López-Mendoza, P.G., Blanco Y Correa, J.M., Ontiveros-Cuadras, J.F., Osti Saenz, J., Reyes Castellanos, J.E., 2018. Sediment geochemistry, accumulation rates and forest structure in a large tropical mangrove ecosystem. Wetlands 38 (2), 307–325.
Runge, F., 1999. The opal phytolith inventory of soils in central Africa—quantities, shapes, classification, and spectra. Rev. Palaeobot. Palynol. 107 (1–2), 23–53.
Russell, J.M., Johnson, T.C., 2005. A high-resolution geochemical record from Lake Edward, Uganda Congo and the timing and causes of tropical African drought during the late Holocene. Quat. Sci. Rev. 24 (12–13), 1375–1389.
Ryner, M., Holmgren, K., Taylor, D., 2008. A record of vegetation dynamics and lake level changes from Lake Emakat, northern Tanzania, during the last c. 1200 years. J. Paleolimnol. 40 (2), 583–601.
Sanders, C.J., Smoak, J.M., Waters, M.N., Sanders, L.M., Brandini, N., Patchineelam, S.R., 2012. Organic matter content and particle size modifications in mangrove sediments as responses to sea level rise. Mar. Environ. Res. 77, 150–155.
Santisuk, T., 1983. Taxonomy and distribution of terrestrial trees and shrubs in the mangrove formations in Thailand. Nat. Hist. Bull. Siam Soc. 5 (1), 63–91.

Schreck III, C.J., Semazzi, F.H., 2004. Variability of the recent climate of eastern Africa. Int. J. Climatol.: A Journal of the Royal Meteorological Society 24 (6), 681–701.
Semesi, A.K., 1998. Mangrove management and utilization in eastern Africa. Ambio 27 (8), 620–626.
Smith, T.J., 1992. Forest structure. In: Robertson, A.I., Alongi, D.M. (Eds.), Tropical Mangrove Ecosystems. American Geophysical Union, Washington DC, pp. 101–136.
Smol, J.P., Birks, H.J., Last, W.M., 2001. Tracking Environmental Change Using Lake Sediments: Volume 4: Zoological Indicators. Springer, Netherlands.
Stager, J.C., Cumming, B.F., Meeker, L.D., 2003. A 10,000-year high-resolution diatom record from Pilkington Bay, lake Victoria, East Africa. Quat. Res. 59 (2), 172–181.
Stoetzel, J., 2014. Towards a Swahili Historical Ecology: Phytolith-Based Analysis in Coastal Eastern Africa since AD 600. Doctoral dissertation, University of Virginia.
Strachan, K.L., Finch, J.M., Hill, T., Barnett, R.L., 2014. A late Holocene sea-level curve for the east coast of South Africa. South Afr. J. Sci. 110 (1/2), 1–9.
Sulas, F., Madella, M., 2012. Archaeology at the micro-scale: micromorphology and phytoliths at a Swahili stonetown. Archaeological and Anthropological Sciences 4 (2), 145–159.
Sulas, F., Fleisher, J., Wynne-Jones, S., 2017. Geoarchaeology of urban space in tropical island environments: Songo Mnara, Tanzania. J. Archaeol. Sci. 77, 52–63.
Sulas, F., Kristiansen, S.M., Wynne-Jones, S., 2019. Soil geochemistry, phytoliths and artefacts from an early Swahili daub house, Unguja Ukuu, Zanzibar. J. Archaeol. Sci. 103, 32–45.
Tchounwou, P.B., Yedjou, C.G., Patlolla, A.K., Sutton, D.J., 2012. Heavy metal toxicity and the environment. In: Luch, A. (Ed.), Molecular, Clinical and Environmental Toxicology, vol. 101. Springer, Basel, pp. 133–164.
Thompson, L.G., Mosley-Thompson, E., Davis, M.E., Henderson, K.A., Brecher, H.H., Zagorodnov, V.S., Mashiotta, T.A., Lin, P.-N., Mikhalenko, V.N., Hardy, D.R., Beer, J., 2002. Kilimanjaro Ice core records: evidence of Holocene climate change in tropical Africa. Science 298 (5593), 589–593.
Tierney, J.E., Smerdon, J.E., Anchukaitis, K.J., Seager, R., 2013. Multidecadal variability in East African hydroclimate controlled by the Indian ocean. Nature 493 (7432), 389–392.
Tinner, W., Hu, F.S., 2003. Size parameters, size-class distribution, and area-number relationship of microscopic charcoal: relevance for fire reconstruction. Holocene 13 (4), 499–505.
Umbanhowar, C.E., Shinneman, A.L.C., Tserenkhand, G., Hammon, E.R., Lor, P., Nail, K., 2009. Regional fire history based on charcoal analysis of sediments from nine lakes in western Mongolia. Holocene 19 (4), 611–624.
Verschuren, D., Laird, K.R., Cumming, B.F., 2000. Rainfall and drought in equatorial east Africa during the past 1,100 years. Nature 403 (6768), 410–414.
Waddington, J.C.B., 1969. A Stratigraphic Record of the Pollen Influx to a Lake in the Big Woods of Minnesota, vol. 123. Geological Society of America special Paper, pp. 263–283.
Wang, S., Li, Y., Fan, B., Cao, Y., You, H., Wang, R., Ge, Y., Da, S., She, Z., Zhang, Z., Zhang, S., Li, C., 2023. Middle to late Holocene environmental evolution and sea level change on the west coast of Bohai Bay. Quat. Int. S1040618223002161.
Watson, J.D., 1928. Mangrove forests of the Malay Peninsula. Malay. For. Rec. 6, 1–275.
Weltje, G.J., 1997. End-member modeling of compositional data: numerical-statistical algorithms for solving the explicit mixing problem. Math. Geol. 29 (4), 503–549.
Whitlock, C., Larsen, C., 2001. Charcoal as a fire proxy. Tracking environmental change using lake sediments: terrestrial, algal, and siliceous indicators 75–97.
Woodroffe, S.A., Long, A.J., Milne, G.A., Bryant, C.L., Thomas, A.L., 2015. New constraints on late Holocene eustatic sea-level changes from Mahé, Seychelles. Quat. Sci. Rev. 115, 1–16.
Wynne-Jones, S., 2013. The public life of the Swahili stonehouse, 14th–15th centuries AD. J. Anthropol. Archaeol. 32 (4), 759–773.
Wynne-Jones, S., Fleisher, J., 2015. Conservation, community archaeology, and archaeological mediation at Songo Mnara, Tanzania. J. Field Archaeol. 40 (1), 110–119.
Wynne-Jones, S., LaViolette, A. (Eds.), 2017. The Swahili World. Routledge.
Zabel, M., Schneider, R.R., Wagner, T., Adegbie, A.T., de Vries, U., Kolonic, S., 2001. Late Quaternary climate changes in Central Africa as inferred from terrigenous input to the Niger Fan. Quat. Res. 56 (2), 207–217.